

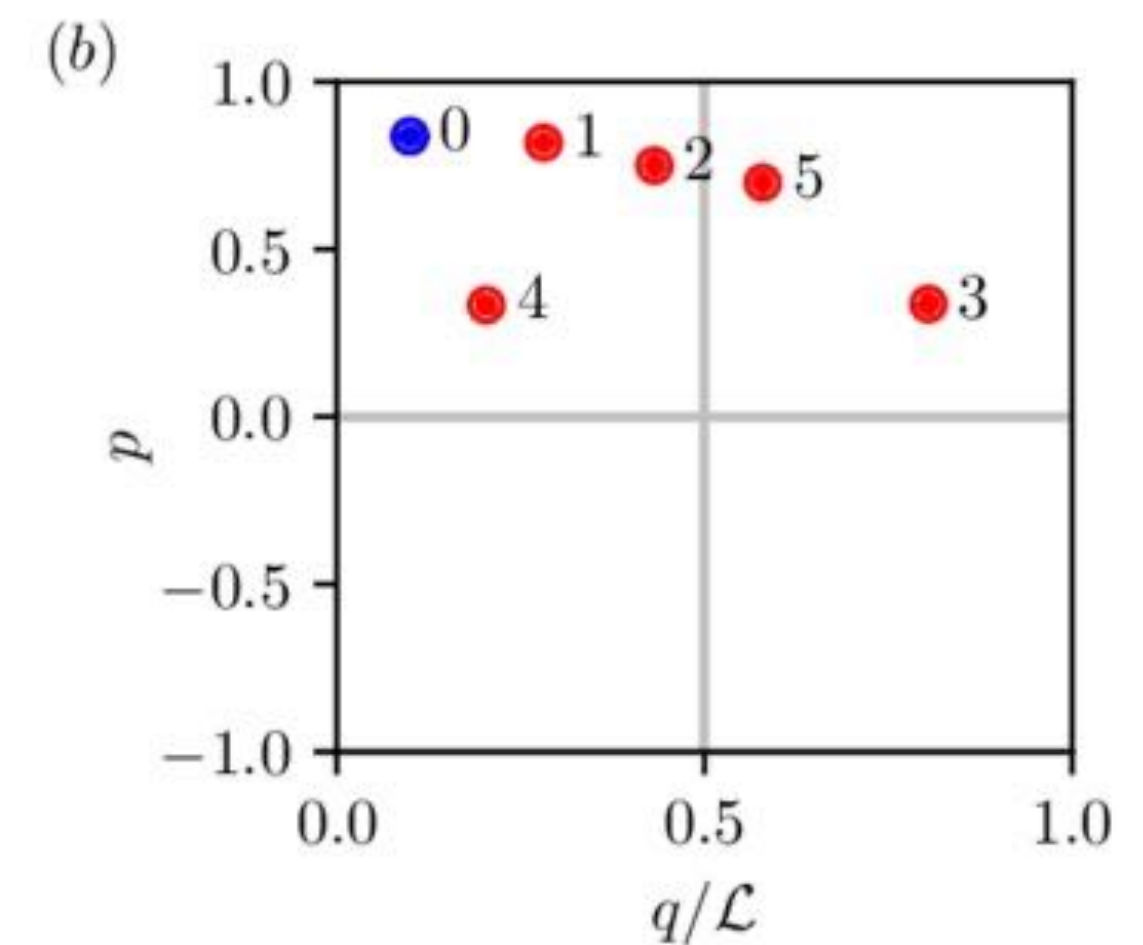
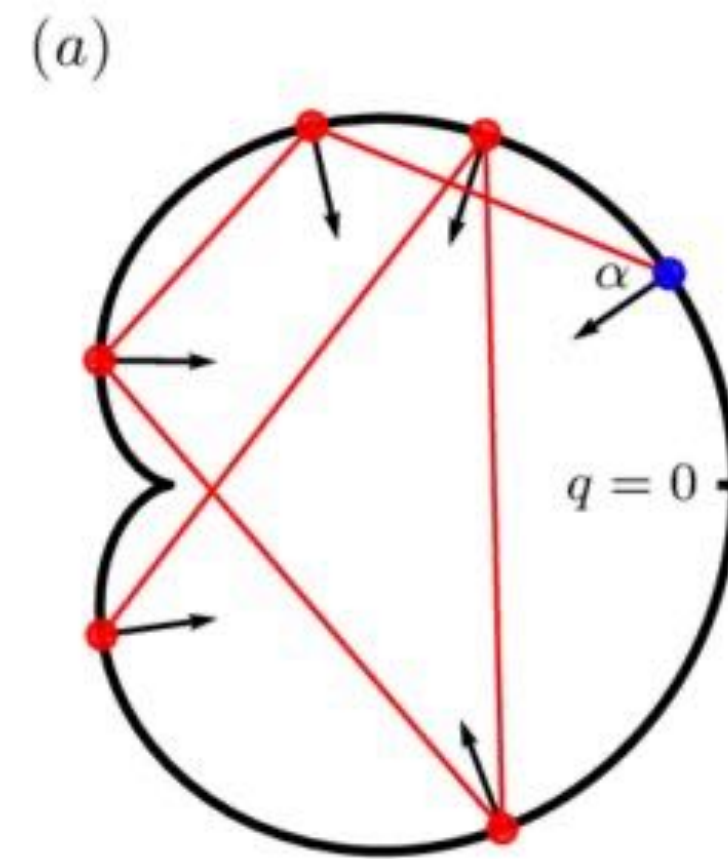
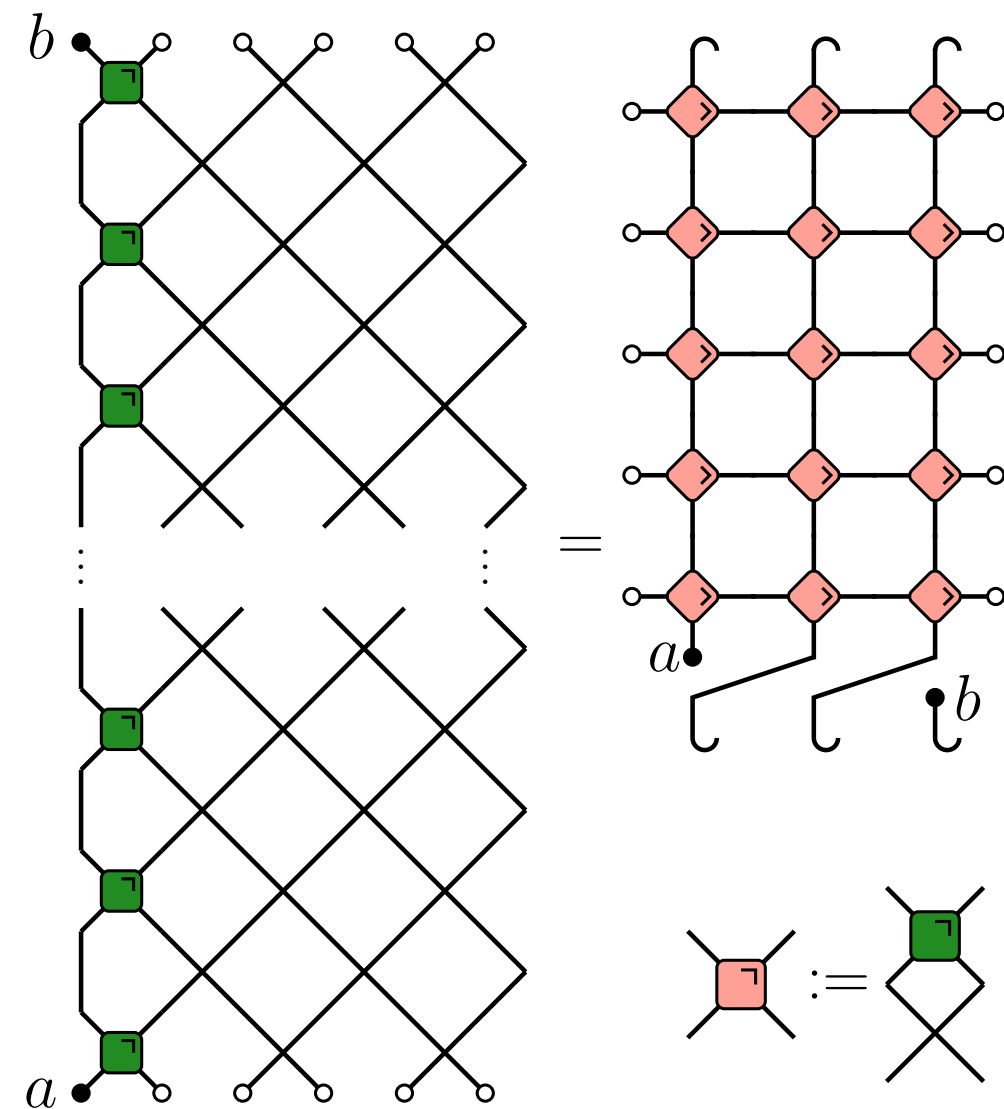
BOUNDARY CHAOS

Tomaž Prosen, University of Ljubljana,

ICTS Bangalore, Jan 23, 2024



Is there an analogy to *Poincare map reduction* in quantum many-body dynamics?



[From, Lozej, PhD Thesis 2020]

References:

F. Fritzsche and TP, Phys. Rev. E106, 014210 (2022)

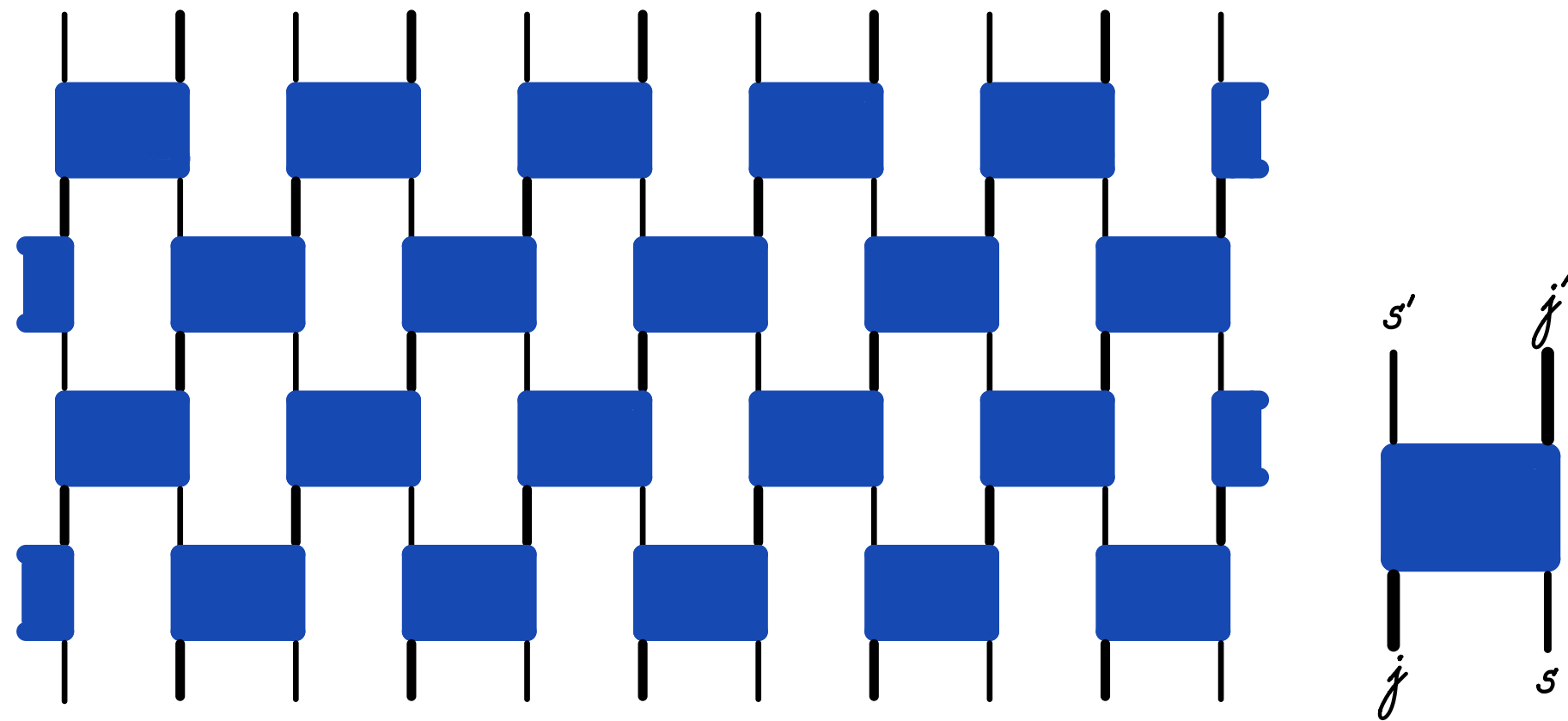
F. Fritzsche, R. Ghosh, and TP, SciPost Physics 15, 092 (2023)



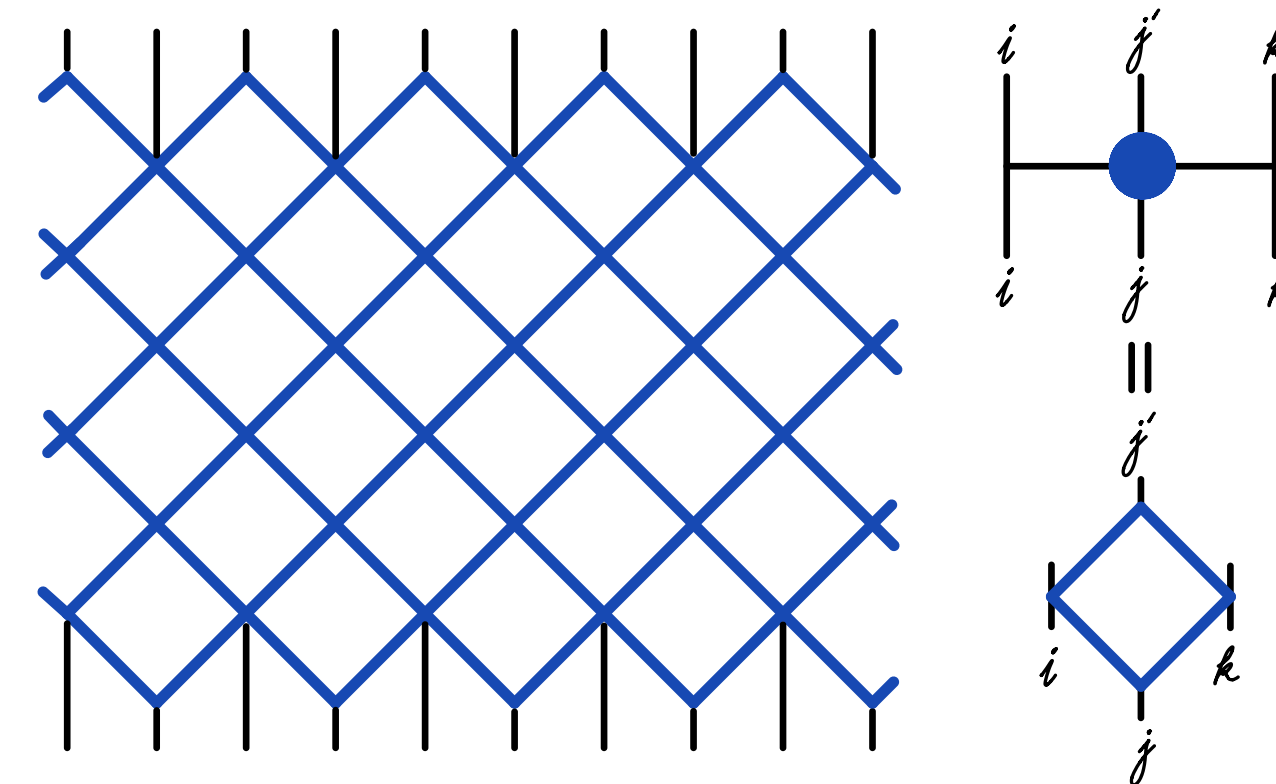
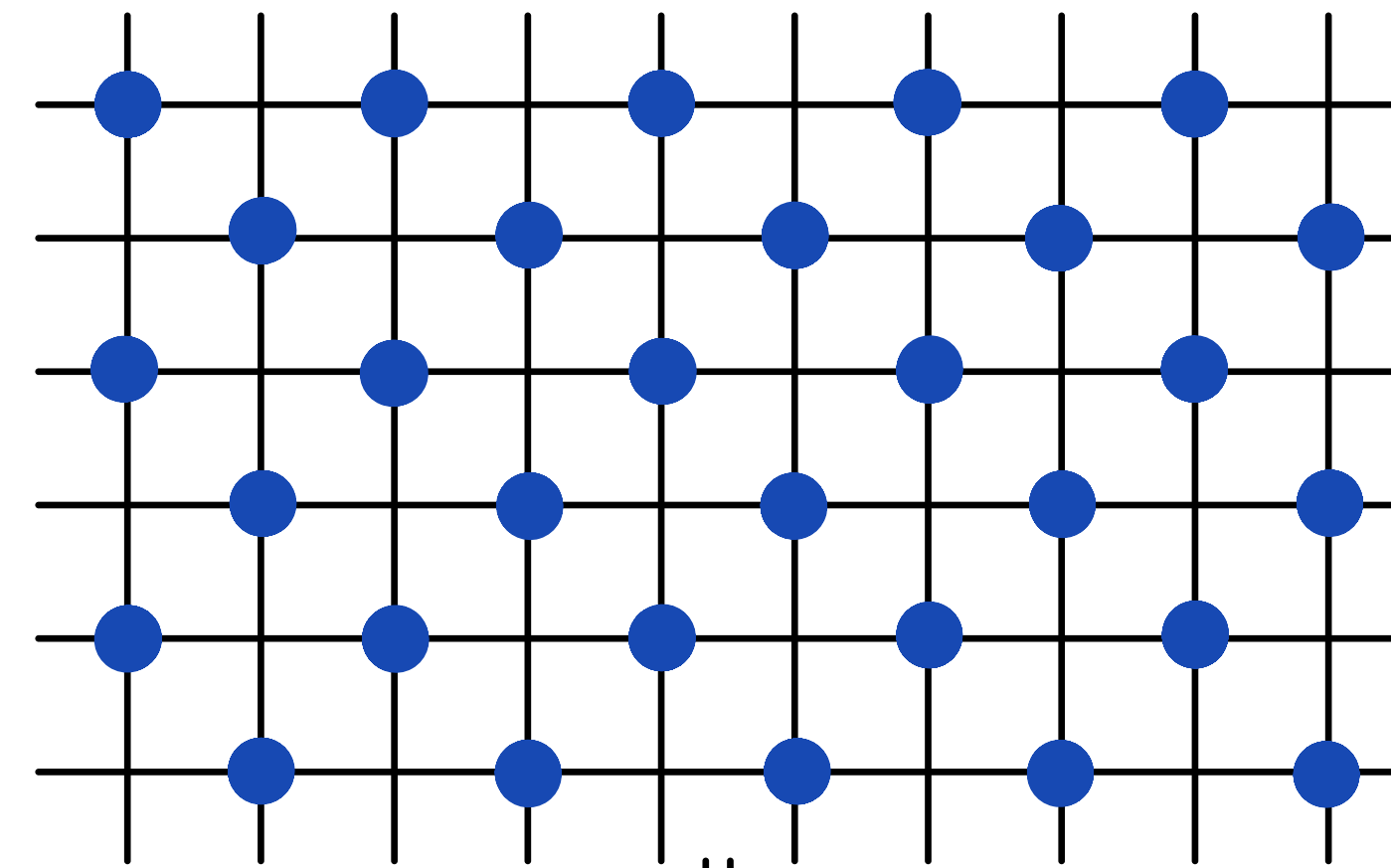
Solvable paradigms of quantum many body dynamics?

**So far, beyond Integrability and Random Systems,
only one game in town: DUAL UNITARY CIRCUITS**

Brickwork vs. IRF unitary circuits



$$U^{\text{br}} = \sum_{j,j'=1}^d \sum_{s,s'=1}^{d'} U_{js}^{s'j'} |s'\rangle \otimes |j'\rangle \langle j| \otimes \langle s|$$



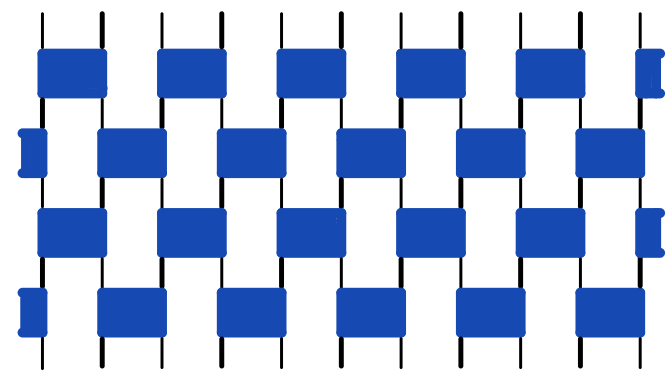
$$U^{\text{IRF}} = \sum_{i,j,k,j'=1}^d (u_{ik})_j^{j'} |i\rangle \otimes |j'\rangle \otimes |k\rangle \langle i| \otimes \langle j| \otimes \langle k|$$

Brickwork

vs.

IRF unitary circuits

$$U^{\text{br}} = \sum_{j,j'=1}^d \sum_{s,s'=1}^{d'} U_{js}^{s'j'} |s'\rangle \otimes |j'\rangle \langle j| \otimes \langle s|$$

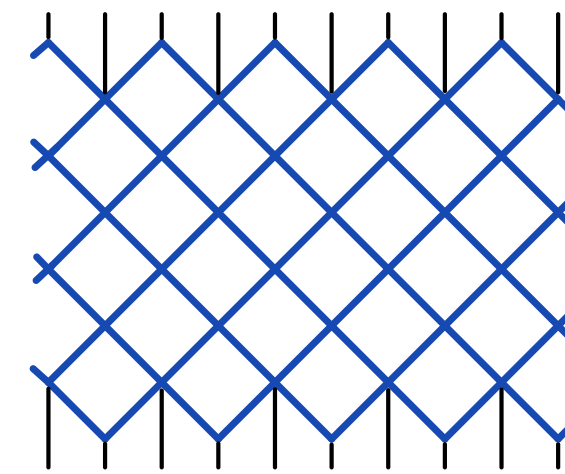


$$\mathcal{U}^e = \prod_{x=1}^L U_{2x-1,2x}^{\text{br}}$$

$$\mathcal{U}^o = \prod_{x=1}^L U_{2x,2x+1}^{\text{br}}$$

$$\mathcal{U} = \mathcal{U}^o \mathcal{U}^e$$

$$U^{\text{IRF}} = \sum_{i,j,k,j'=1}^d (u_{ik})_j^{j'} |i\rangle \otimes |j'\rangle \otimes |k\rangle \langle i| \otimes \langle j| \otimes \langle k|$$



$$\mathcal{U}^e = \prod_{x=1}^L U_{2x-1,2x,2x+1}^{\text{IRF}}$$

$$\mathcal{U}^o = \prod_{x=1}^L U_{2x,2x+1,2x+2}^{\text{IRF}}$$

Gauge symmetry:

$$U^{\text{br}} \leftarrow (h^\dagger \otimes g^\dagger) U^{\text{br}} (g \otimes h)$$

$$G^{\text{br}} = \text{SU}(d) \otimes \text{SU}(d')$$

$$U^{\text{IRF}} \leftarrow (\Delta^\dagger \otimes g^\dagger \otimes \Delta^\dagger) U^{\text{IRF}} (\Delta \otimes g \otimes \Delta)$$

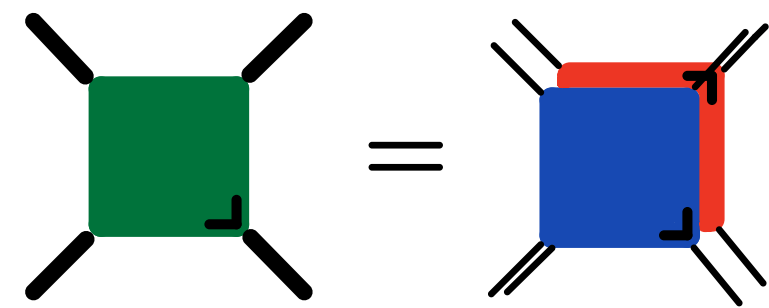
$$G^{\text{IRF}} = \text{SU}(d) \otimes \text{U}(1)^{\otimes (d-1)}$$

Folded circuit representation of correlation functions

Brickwork circuits

$$C_{a,b}(x,y;t) = \lim_{L \rightarrow \infty} \frac{1}{\dim \mathcal{H}} \text{tr}(a_x \mathcal{U}^t b_y \mathcal{U}^{-t}) = \lim_{L \rightarrow \infty} \langle\langle b_y | \mathcal{W}^t | a_x \rangle\rangle$$

$$W^{\text{br}} = U^{\text{br}} \otimes (U^{\text{br}})^T$$

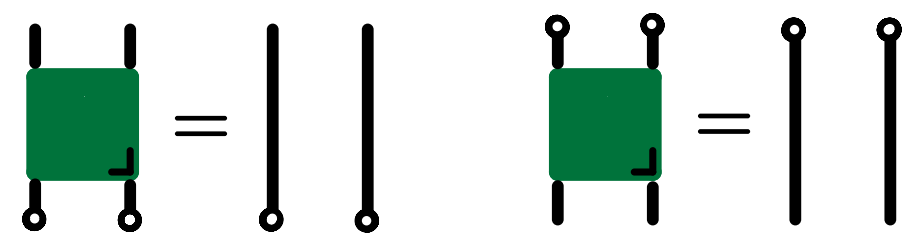


$$\parallel = \text{!}$$

$$|a\rangle\rangle = \frac{1}{\sqrt{d}} \sum_{i,j} a_i^j |i\rangle \otimes |j\rangle$$

$$|b\rangle\rangle = \frac{1}{\sqrt{d}} \sum_{i,j} b_i^j |i\rangle \otimes |j\rangle$$

$$|o\rangle\rangle = \frac{1}{\sqrt{d}} \sum_i |i\rangle \otimes |i\rangle,$$



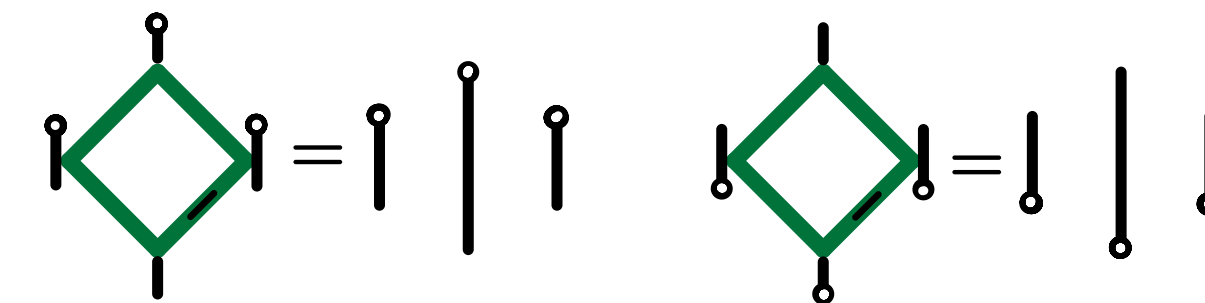
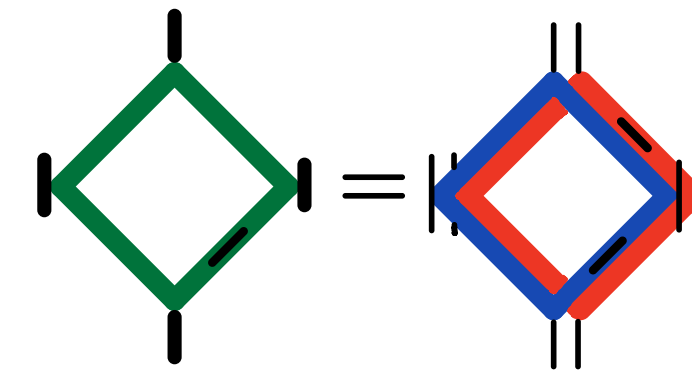
Unitarity:

$$W^{\text{br}} |o\rangle\rangle \otimes |o\rangle\rangle = |o\rangle\rangle \otimes |o\rangle\rangle$$

$$\langle\langle o| \otimes \langle\langle o| W^{\text{br}} = \langle\langle o| \otimes \langle\langle o|$$

IRF circuits

$$W^{\text{IRF}} = U^{\text{IRF}} \otimes (U^{\text{IRF}})^T$$



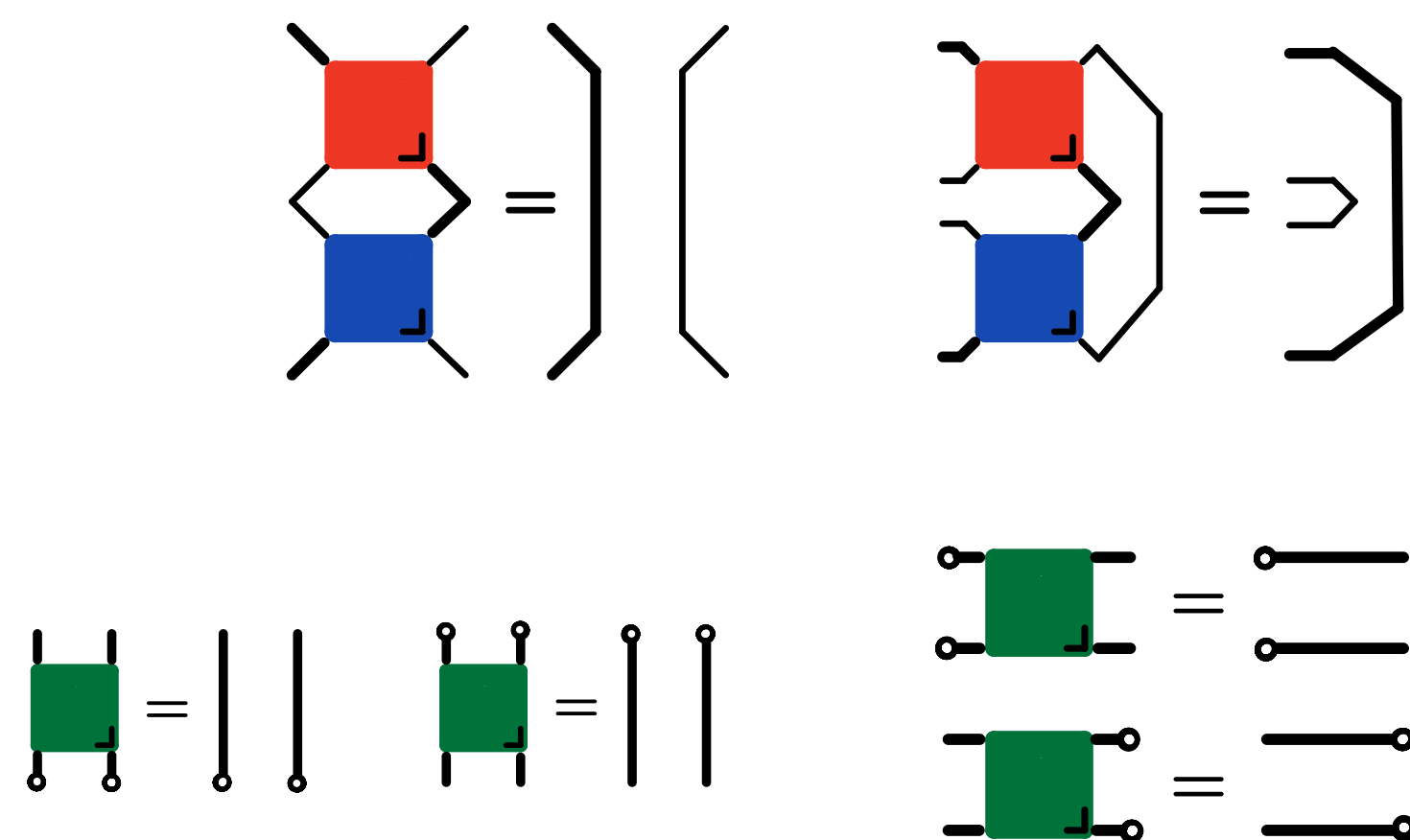
$$W^{\text{IRF}} |o\rangle\rangle \otimes |o\rangle\rangle \otimes |o\rangle\rangle = |o\rangle\rangle \otimes |o\rangle\rangle \otimes |o\rangle\rangle$$

$$\langle\langle o| \otimes \langle\langle o| \otimes \langle\langle o| W^{\text{IRF}} = \langle\langle o| \otimes \langle\langle o| \otimes \langle\langle o|$$

Dual Unitarity

Brickwork circuits

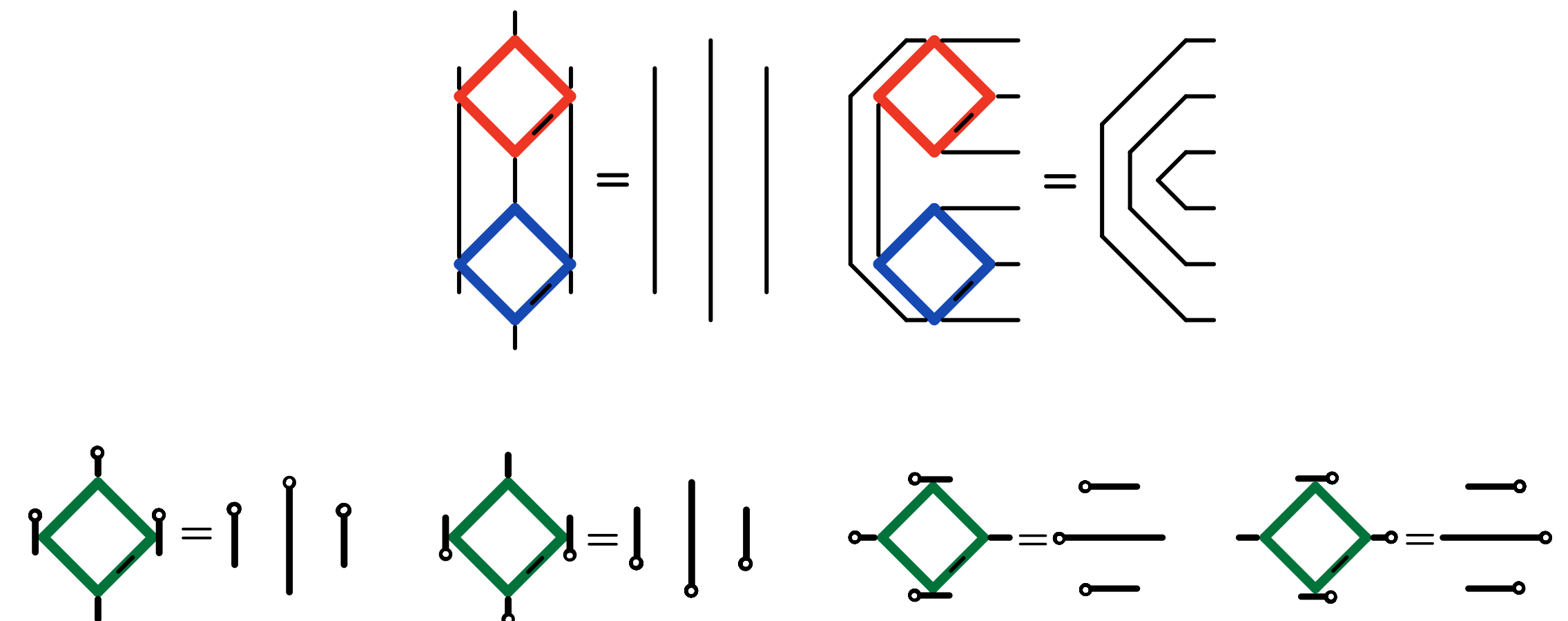
$$\tilde{U}^{\text{br}} = \sum_{j,j'=1}^d \sum_{s,s'=1}^{d'} U_{js'}^{sj'} |s'\rangle \otimes |j'\rangle \langle j| \otimes \langle s|$$



IRF circuits

$$\tilde{U}^{\text{IRF}} = \sum_{i,j,k,j'=1}^d (u_{jj'})_i^k |i\rangle \otimes |j'\rangle \otimes |k\rangle \langle i| \otimes \langle j| \otimes \langle k|$$

$$(\tilde{u}_{jj'})_i^k := (u_{ik})_j^{j'}$$



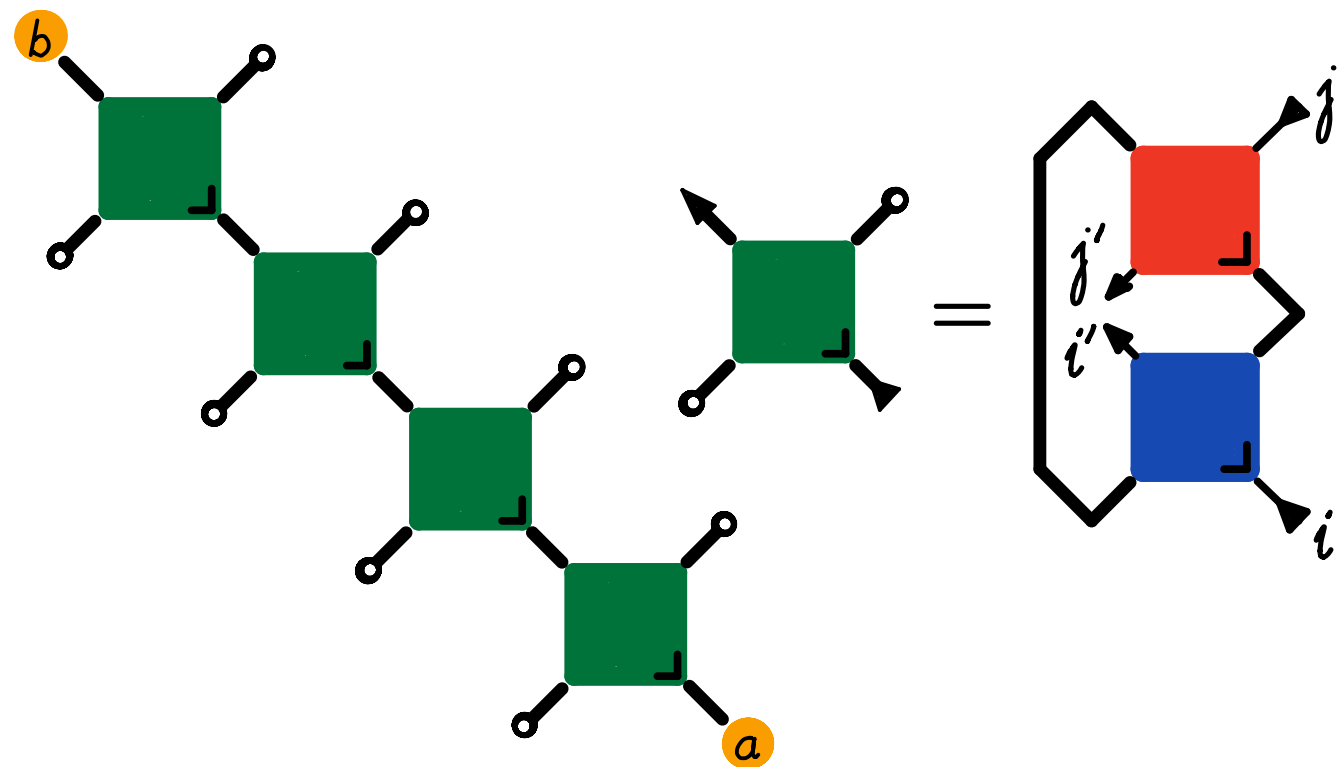
Dual unitarity and exact channel repr. of dynamical correlators

Brickwork circuits

$$C_{a,b}(x,y;t) = \delta_{y,x+2t} \delta_{\text{mod}(x,2),1} \text{tr}(b \mathcal{M}_+^{2t}(a)) + \delta_{y,x-2t} \delta_{\text{mod}(x,2),0} \text{tr}(b \mathcal{M}_-^{2t}(a))$$

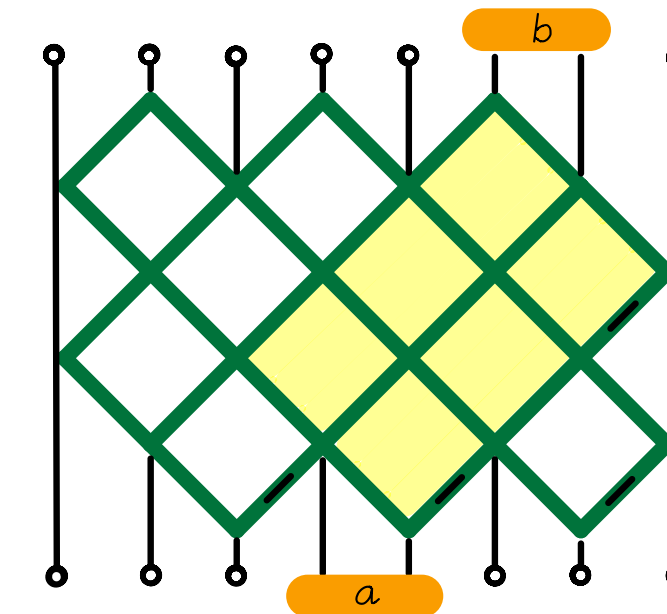
$$\mathcal{M}_+(a) = \frac{1}{d'} (\text{tr} \otimes \mathbb{I}) \left((U^{\text{br}})^\dagger (a \otimes \mathbb{1}) U^{\text{br}} \right)$$

$$\mathcal{M}_-(a) = \frac{1}{d} (\mathbb{I} \otimes \text{tr}) \left((U^{\text{br}})^\dagger (\mathbb{1} \otimes a) U^{\text{br}} \right)$$



[Bertini, Kos, TP, PRL'19]

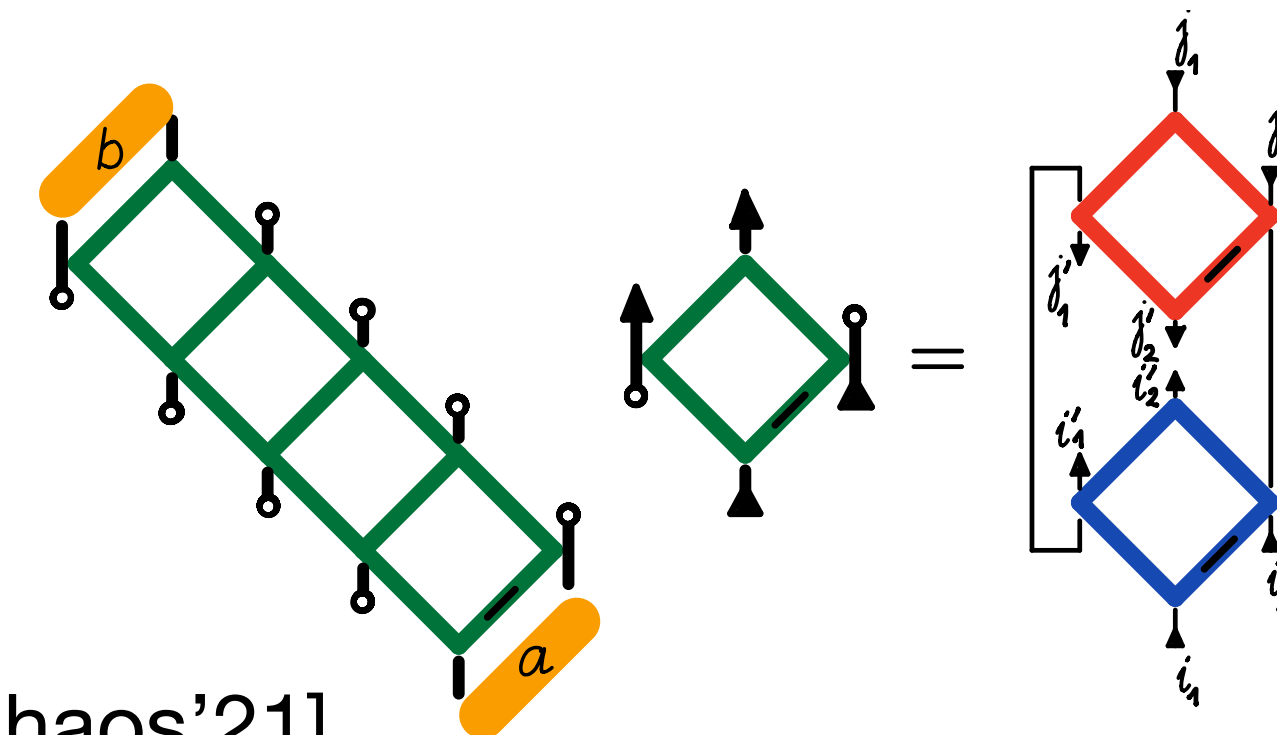
IRF circuits



$$C_{a,b}(x,y;t) = \delta_{y,x+2t} \delta_{\text{mod}(x,2),1} \text{tr}(b \mathcal{K}_+^{2t}(a)) + \delta_{y,x-2t} \delta_{\text{mod}(x,2),0} \text{tr}(b \mathcal{K}_-^{2t}(a))$$

$$\mathcal{K}_+(a) = \frac{1}{d} (\text{tr} \otimes \mathbb{I} \otimes \mathbb{I}) \left((U^{\text{IRF}})^\dagger (a \otimes \mathbb{1}) U^{\text{IRF}} \right)$$

$$\mathcal{K}_-(a) = \frac{1}{d} (\mathbb{I} \otimes \mathbb{I} \otimes \text{tr}) \left((U^{\text{IRF}})^\dagger (\mathbb{1} \otimes a) U^{\text{IRF}} \right)$$

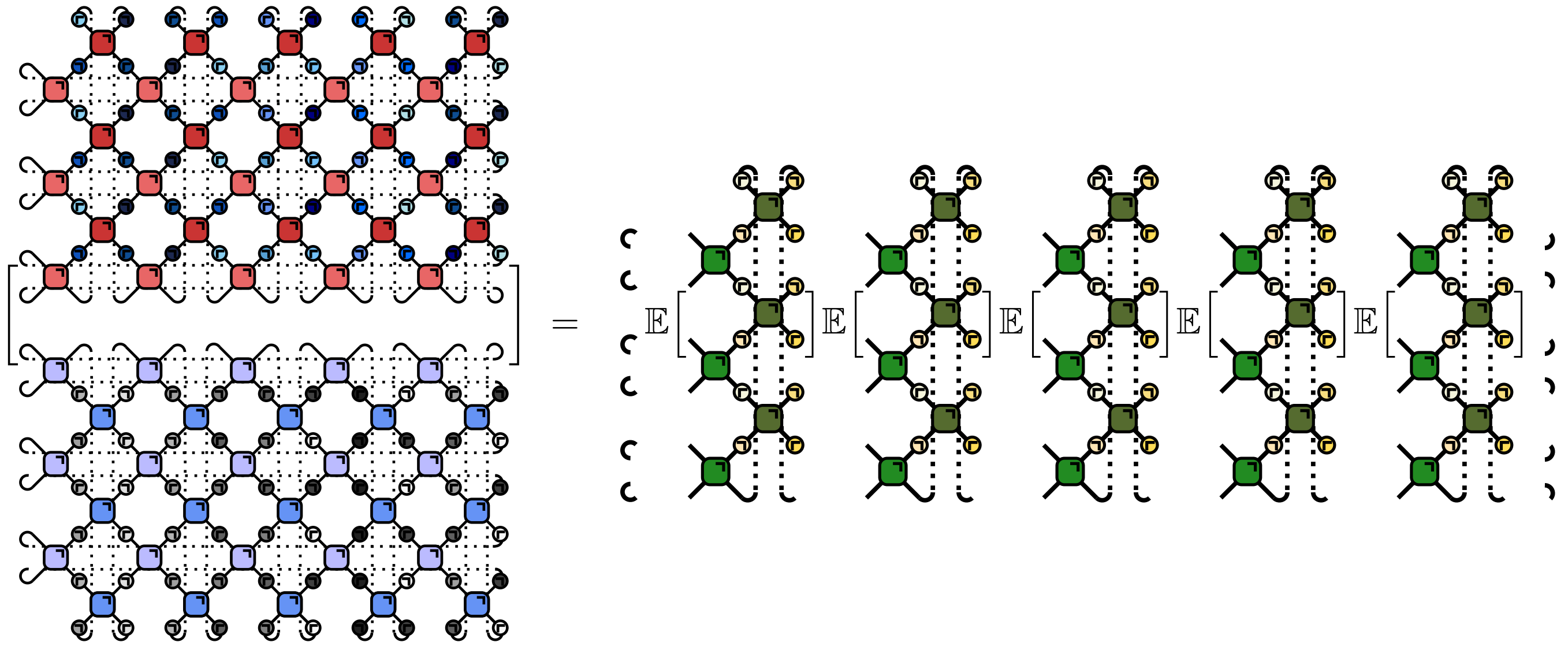


[TP, Chaos'21]

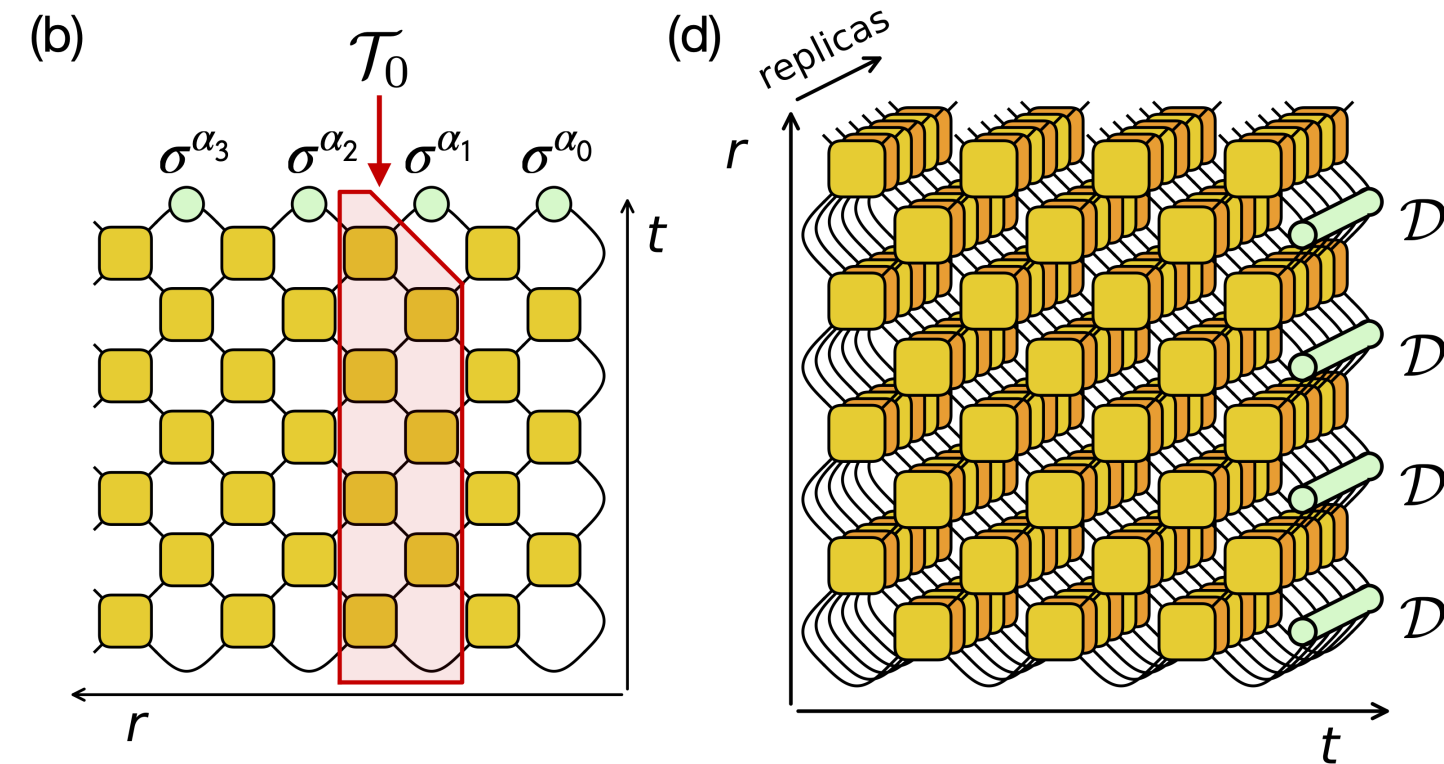
Nontrivial results and applications of dual unitary circuits

Exact RMT ramp of SFF
 [Bertini, Kos, P, PRL'18, CMP'21]:

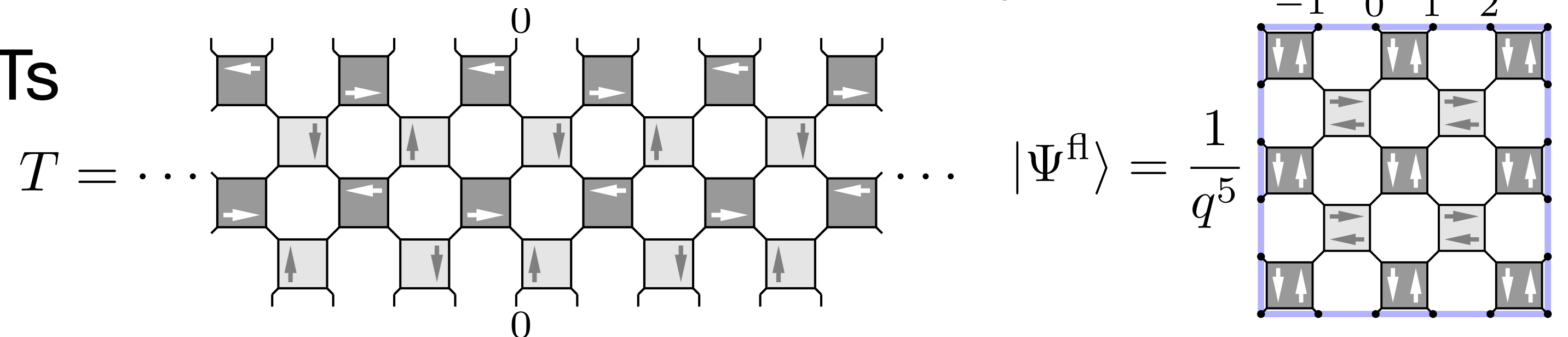
$$K(t, L) = \mathbb{E} \left[\text{tr}(U_L)^t \text{tr}(U_L^\dagger)^t \right] = \mathbb{E} \left[\dots \right]$$



Exact emergent quantum state design
 and exact projected ensemble/deep
 thermalization [Ho, Choi, PRL'22,
 Ippoliti, Ho, arXiv:2204.13657]



Discrete holography, discrete CFTs
 [Masanes, arXiv:2301.02825]



But here we will discuss even much simpler many-body dynamics, where interactions are confined to system's boundaries...

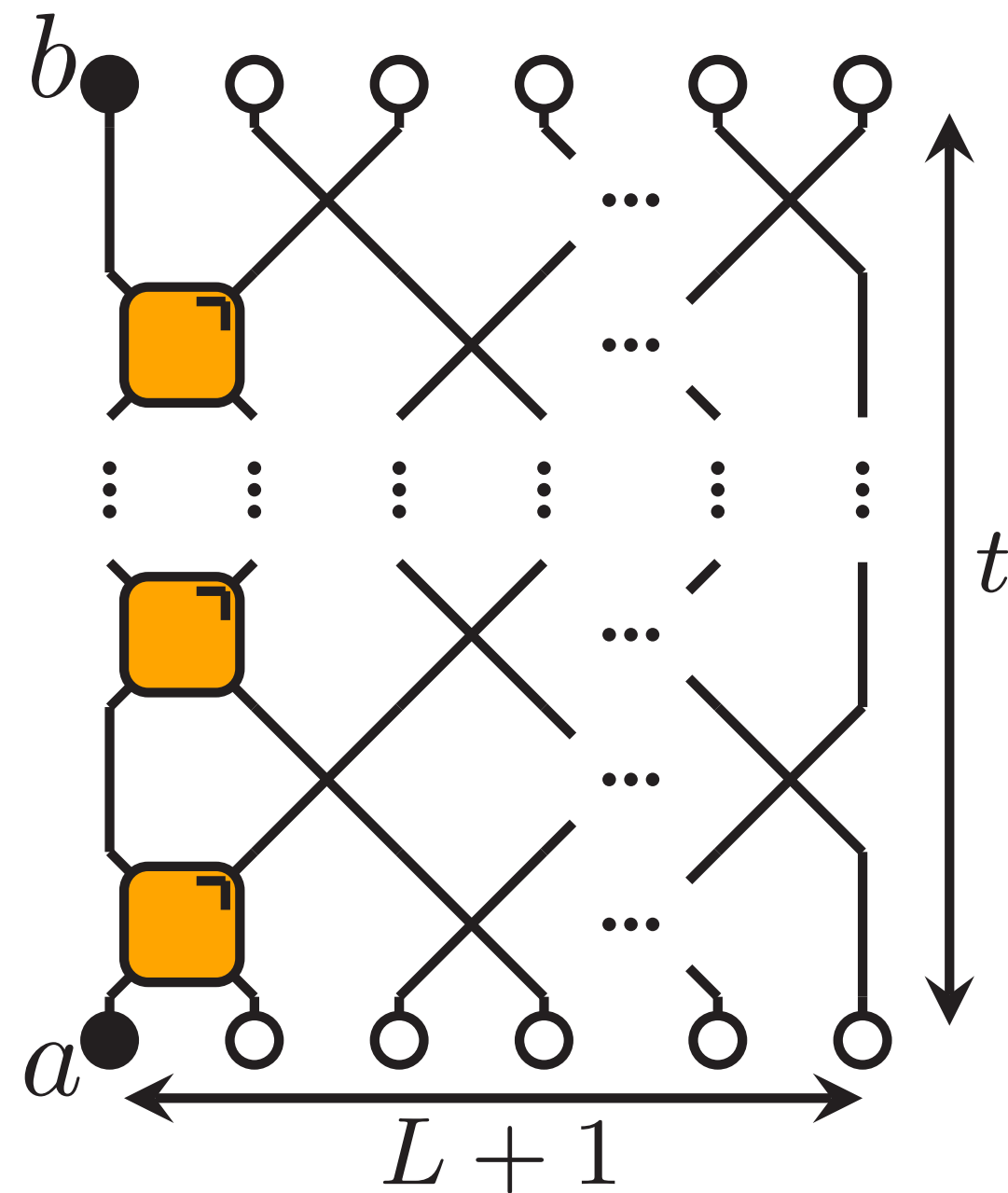
Boundary Chaos Circuit

$$\mathcal{U} = \mathcal{U}_2 \mathcal{U}_1 \quad \mathcal{U}_1 = \prod_{i=1}^{\lfloor L/2 \rfloor} P_{2i-1, 2i}, \quad \mathcal{U}_2 = U_{0,1} \prod_{i=1}^{\lfloor (L-1)/2 \rfloor} P_{2i, 2i+1},$$

$$C_{ab}(t) = \frac{1}{N} \text{tr}(\mathcal{U}^{-t} a_0 \mathcal{U}^t b_0)$$

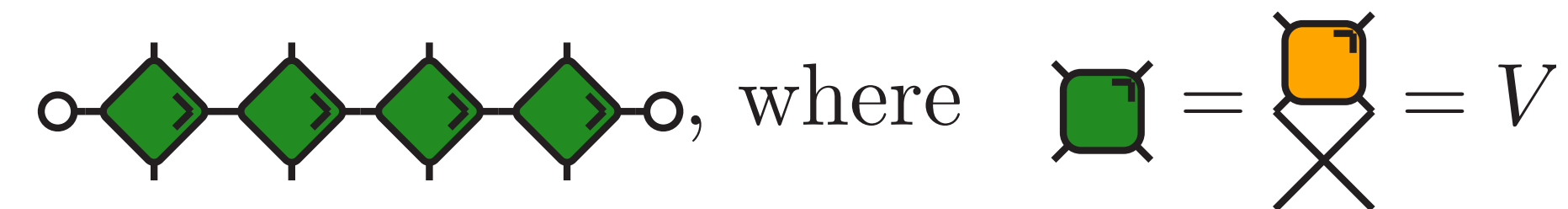
$$\mathcal{W} = \mathcal{W}_1 \mathcal{W}_2 \quad \mathcal{W}_2 = W_{0,1} \prod_i S_{2i, 2i+1}, \quad \mathcal{W}_1 = \prod_i S_{2i-1, 2i},$$

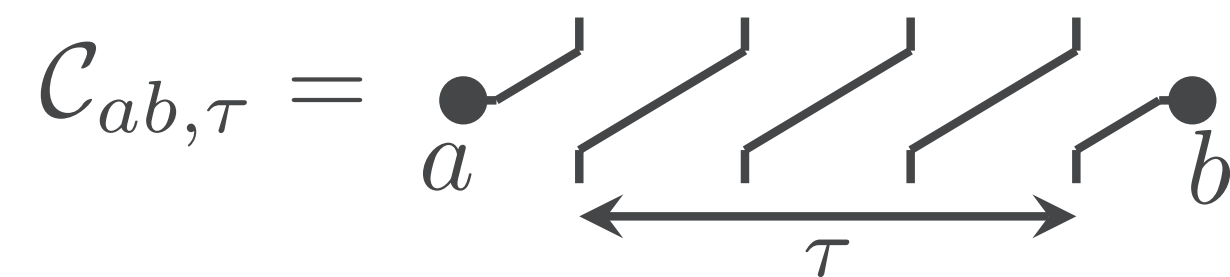
$$C_{ab}(t) = \langle b_0 | \mathcal{W}^t | a_0 \rangle =$$



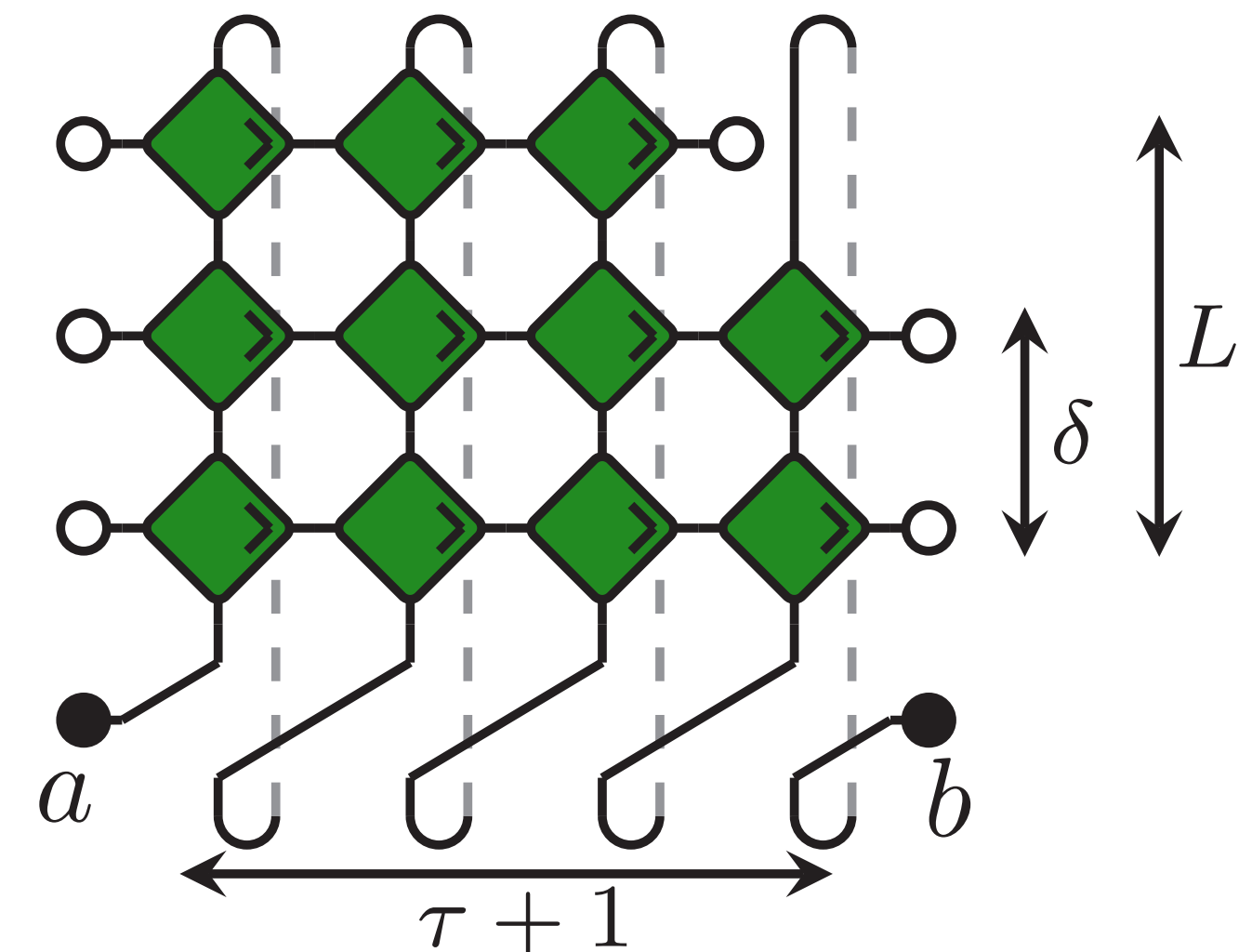
Boundary circuit to Helical tensor network mapping

$$t = L\tau + \delta$$

$$\mathcal{T}_\tau = \text{---} \diamond \text{---} \diamond \text{---} \diamond \text{---} \diamond \text{---} \text{---}, \text{ where } \text{---} \square \text{---} = \text{---} \square \text{---} = V$$


$$\mathcal{C}_{ab,\tau} = \text{---} \bullet \text{---} \text{---} \text{---} \text{---} \text{---} \text{---} \text{---} \bullet \text{---} \text{---}$$


$$\mathcal{C}_{ab}(t) = \text{tr}([\mathcal{T}_\tau^{L-\delta} \otimes \mathbb{1}_{q^2}] \mathcal{T}_{\tau+1}^\delta \mathcal{C}_{ab,\tau+1}) =$$



Computation of correlators are easy for $t \sim L$ iterating the transfer matrix!

Unitality and identity preservation of the operator gate (both consequence of unitarity of the impurity gate):

$$\begin{array}{c} \text{---} \\ \diagup \quad \diagdown \\ \text{---} \end{array} = \begin{array}{c} \circ \\ | \\ \circ \end{array} \begin{array}{c} \circ \\ | \\ \circ \end{array} \quad \text{and} \quad \begin{array}{c} \circ \\ \diagdown \quad \diagup \\ \text{---} \end{array} = \begin{array}{c} \circ \\ | \\ \circ \end{array} \begin{array}{c} \circ \\ | \\ \circ \end{array}$$

imply trivial eigenvalue $1 \in \text{spec}(\mathcal{T}_\tau)$ with eigenvector $|\circ\rangle^{\otimes \tau}$

Moreover, unitality implies nesting of the spectra of transfer matrices

$$\text{spec}(\mathcal{T}_\tau) \subseteq \text{spec}(\mathcal{T}_{\tau+1})$$

$|r_\lambda, s\rangle = |\circ\rangle^{\otimes s} \otimes |r_\lambda\rangle \otimes |\circ\rangle^{\otimes \rho - \tau - s}$ and for each eigenvalue there is an integer τ_λ : $\lambda \in \text{spec}(\mathcal{T}_{\tau_\lambda})$ but $\lambda \notin \text{spec}(\mathcal{T}_{\tau_\lambda - 1})$

T-dual impurity gate

Impurity gate U being T-dual (unitary partial transpose) is equivalent to V being dual-unitary

In this case, all $|r_\lambda, s\rangle = |o\rangle^{\otimes s} \otimes |r_\lambda\rangle \otimes |o\rangle^{\otimes \rho - \tau - s}$ are proper eigenvectors of \mathcal{T}_τ with eigenspace projectors

$$\mathcal{P}_{\lambda, \tau} = \sum_{s=0}^{\tau - \tau_\lambda} |r_\lambda, s\rangle \langle l_\lambda, s| \quad \mathcal{T}_\tau = \sum_\lambda \lambda \mathcal{P}_{\lambda, \tau}$$

$$\begin{aligned} C_{ab}(t) &= \sum_{\lambda, \sigma} \lambda^{L-\delta} \sigma^\delta (\langle l_\lambda | \otimes \langle b |) |r_\sigma\rangle \langle l_\sigma | (|a\rangle \otimes |r_\lambda\rangle) \\ &\sim \lambda_1^{L-\delta} \sigma_1^\delta (\langle l_{\lambda_1} | \otimes \langle b |) |r_{\sigma_1}\rangle \langle l_{\sigma_1} | (|a\rangle \otimes |r_{\lambda_1}\rangle) \end{aligned}$$

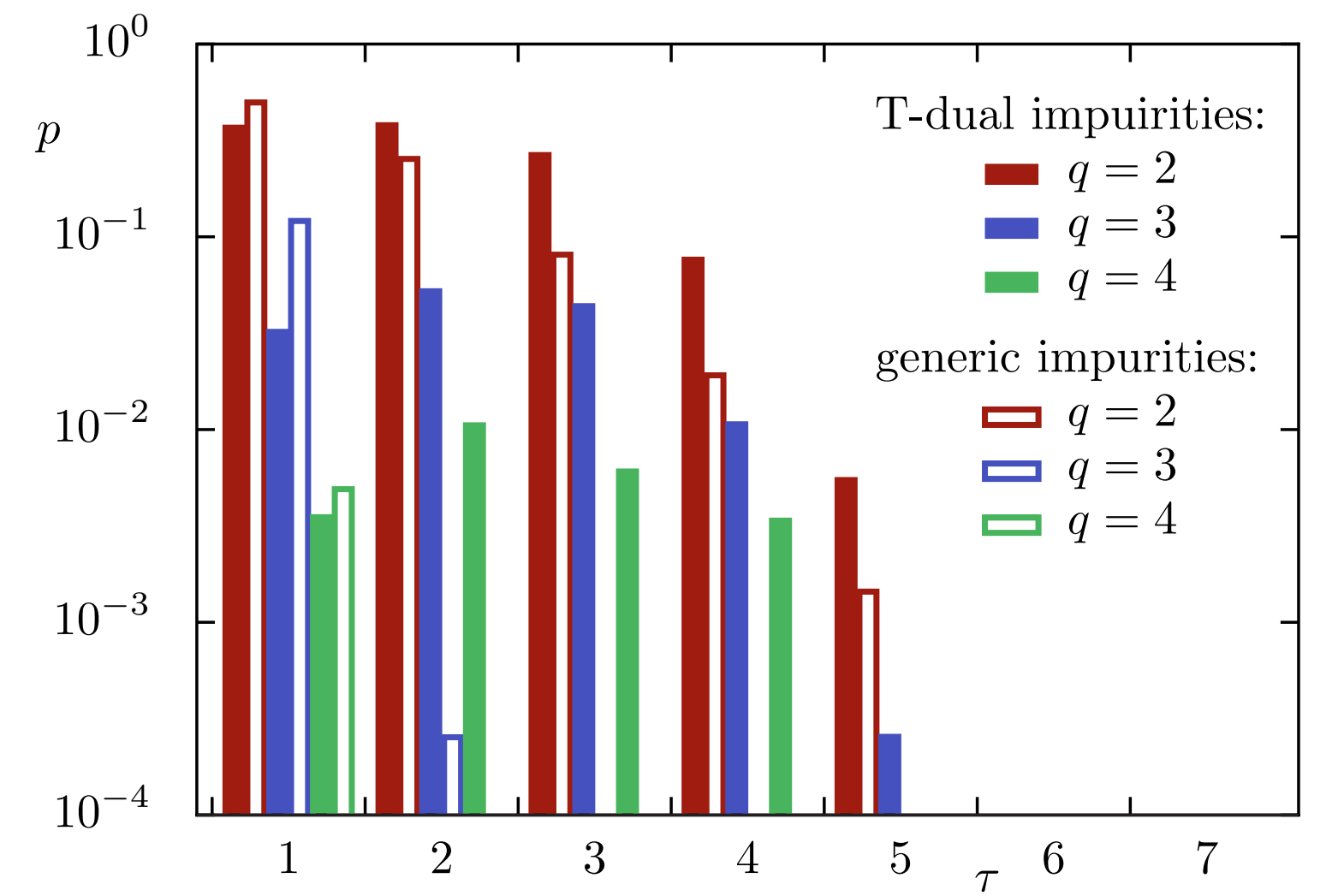
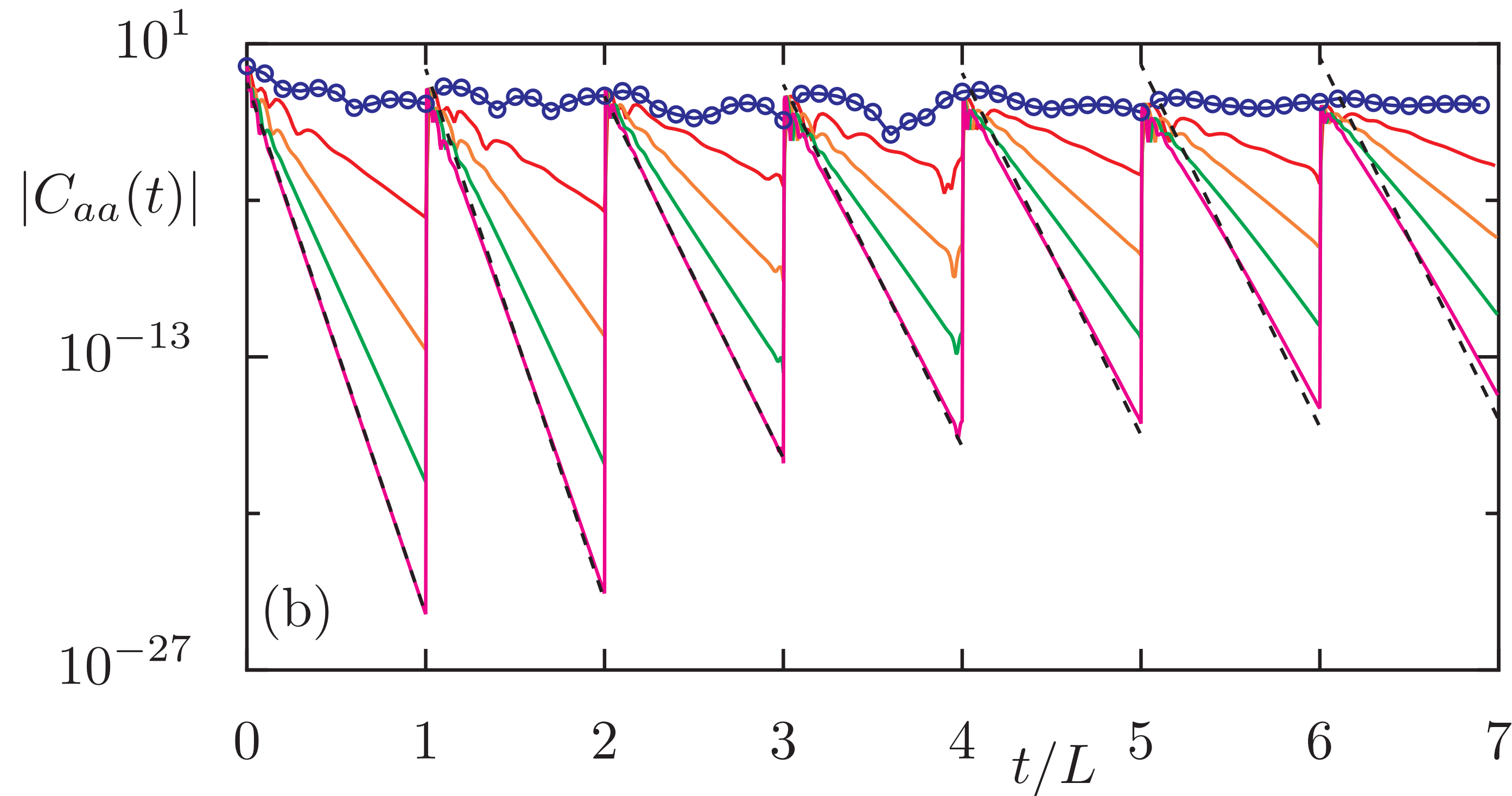
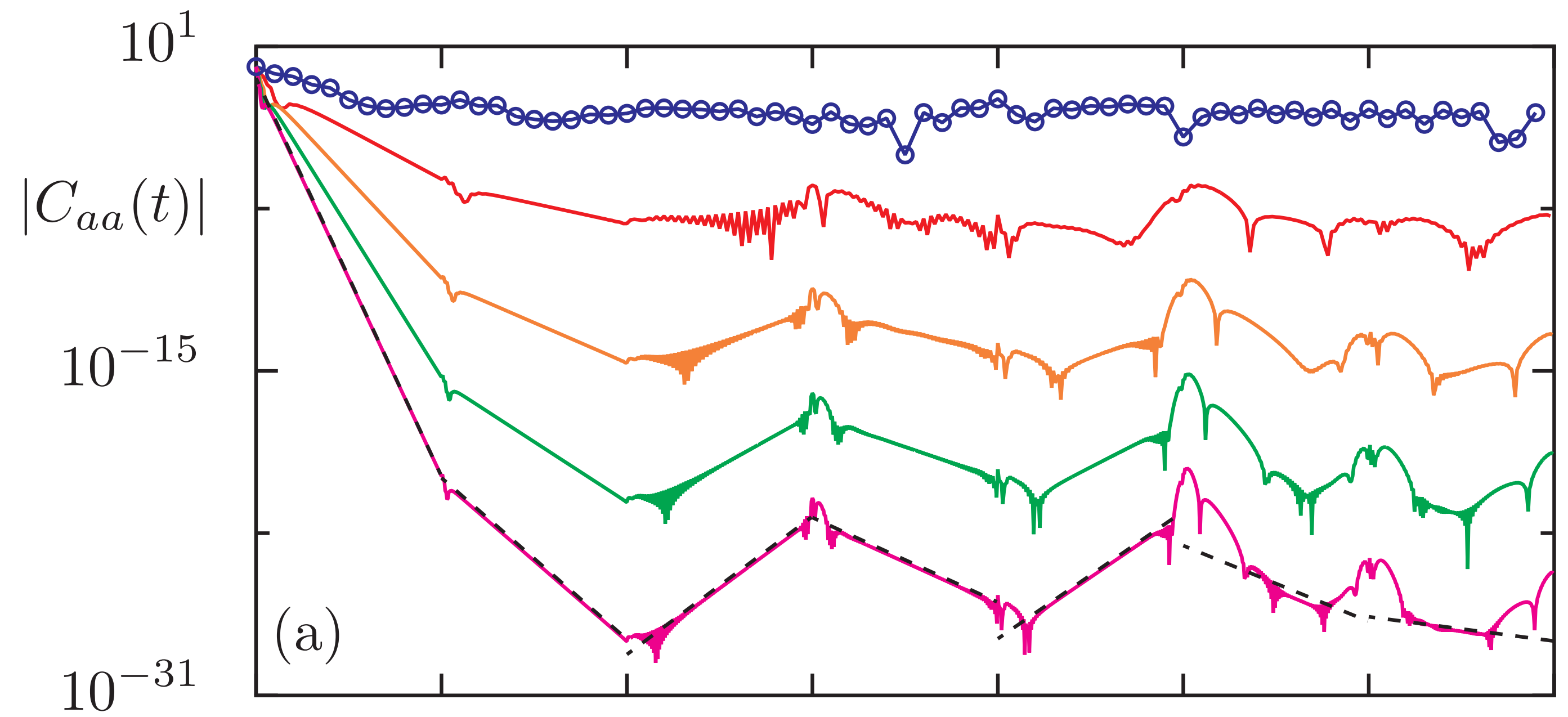


FIG. 3. Probability $p(|\lambda_0(\tau + 1)| > |\lambda_0(\tau)|)$, i.e., for the largest nontrivial eigenvalue to grow when advancing from τ to $\tau + 1$ for various q and for both the T-dual and the generic case. Here we use more than 2000 realizations and 500 for the largest accessible values of τ , respectively, from the same ensembles as used for Fig. 1. The maximum system size is given by $\tau + 1 = 11$, $\tau + 1 = 8$, and $\tau + 1 = 5$ for $q = 2, 3, 4$, respectively. In particular, for $q = 2, 3$ the probability is found to be zero, when there is no bar depicted. For $q = 4$, this holds only up to $\tau = 4$ as we compute the leading eigenvalue only up to $\tau + 1 = 5$.

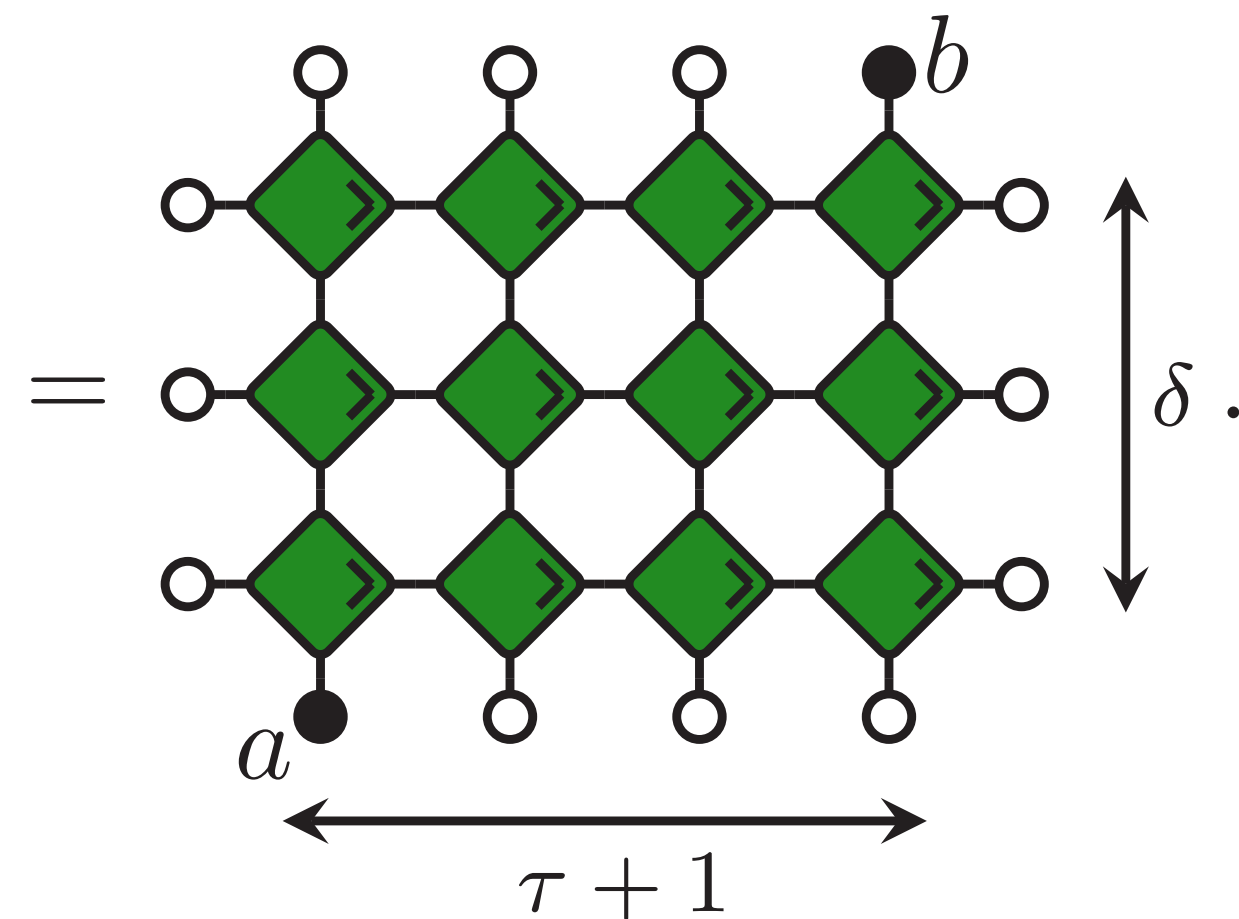
Generic impurity gate

\mathcal{T}_τ ceases to be diagonalizable; has Jordan blocks of dimension $\tau - \tau_\lambda + 1$

only $\langle l_\lambda, 0 |$ remains a proper left eigenvector (and analogously for the right eigenvector)

Hence, the trivial eigenprojector $|\circ\rangle \langle \circ|^{\otimes \tau}$ (contrary to the T-dual case) does contribute in the leading order:

$$C_{ab}(L\tau + \delta) \sim \langle \circ |^{\otimes \tau} \otimes \langle b | \mathcal{T}_{\tau+1}^\delta | a \rangle \otimes | \circ \rangle^{\otimes \tau}$$



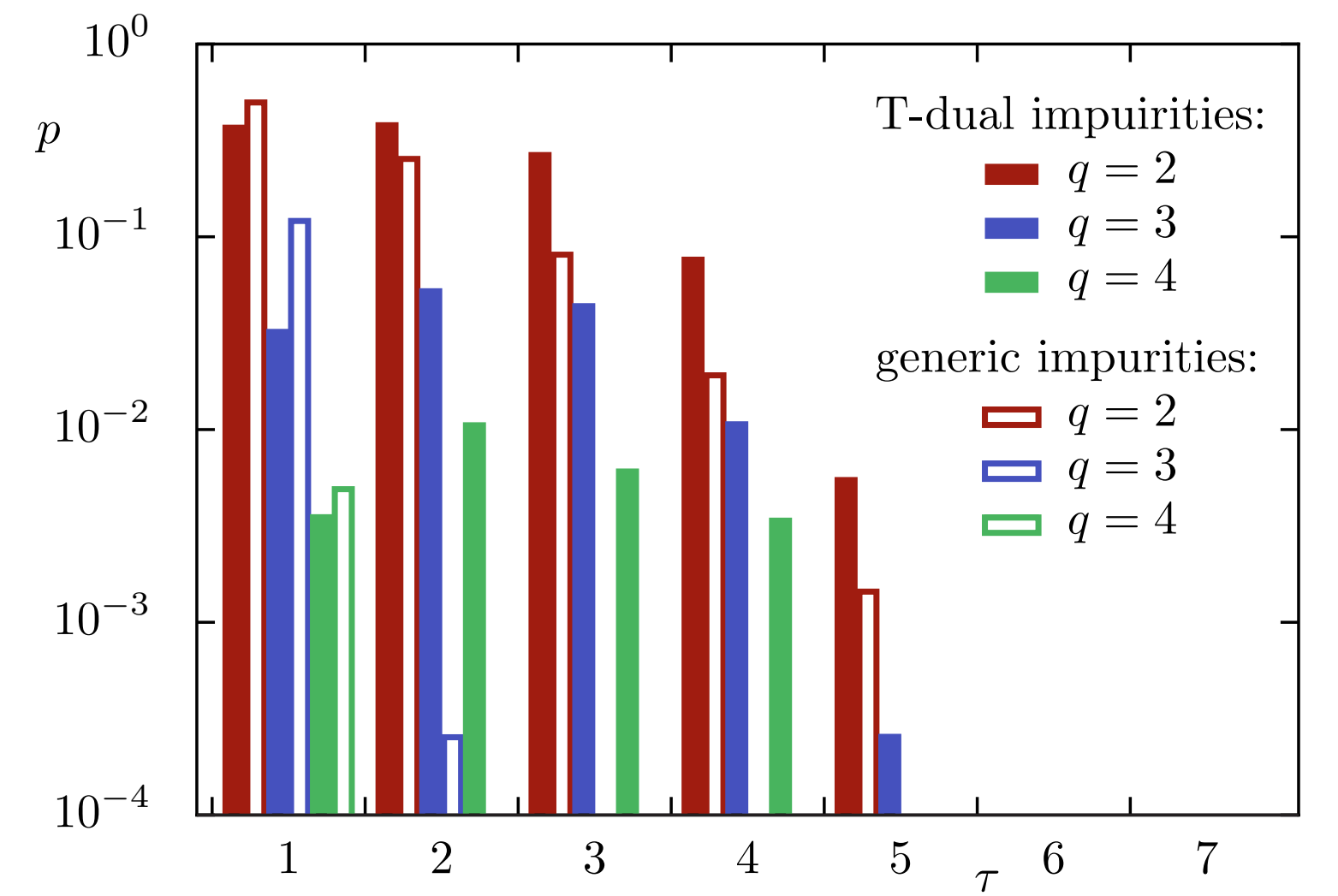
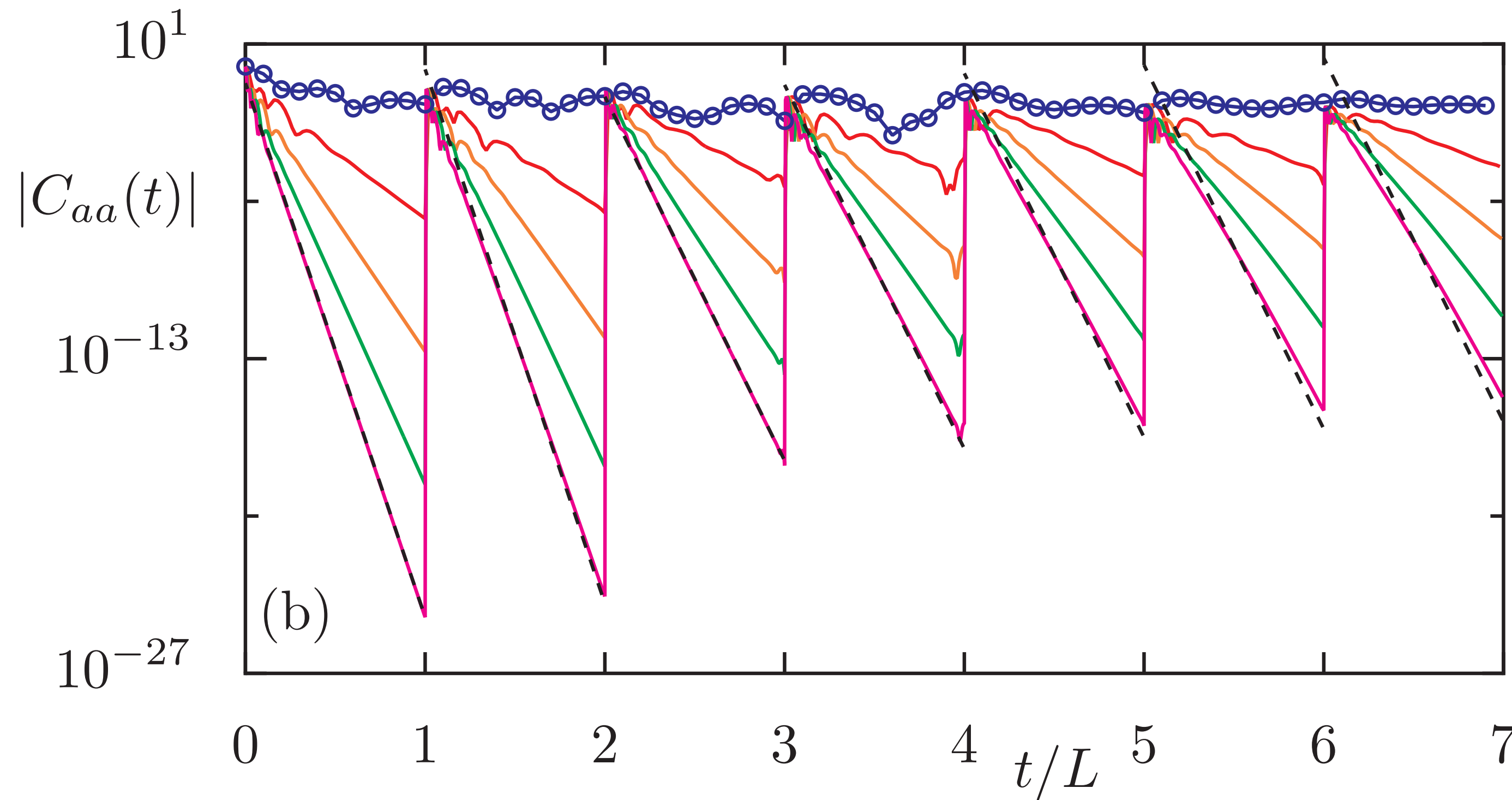
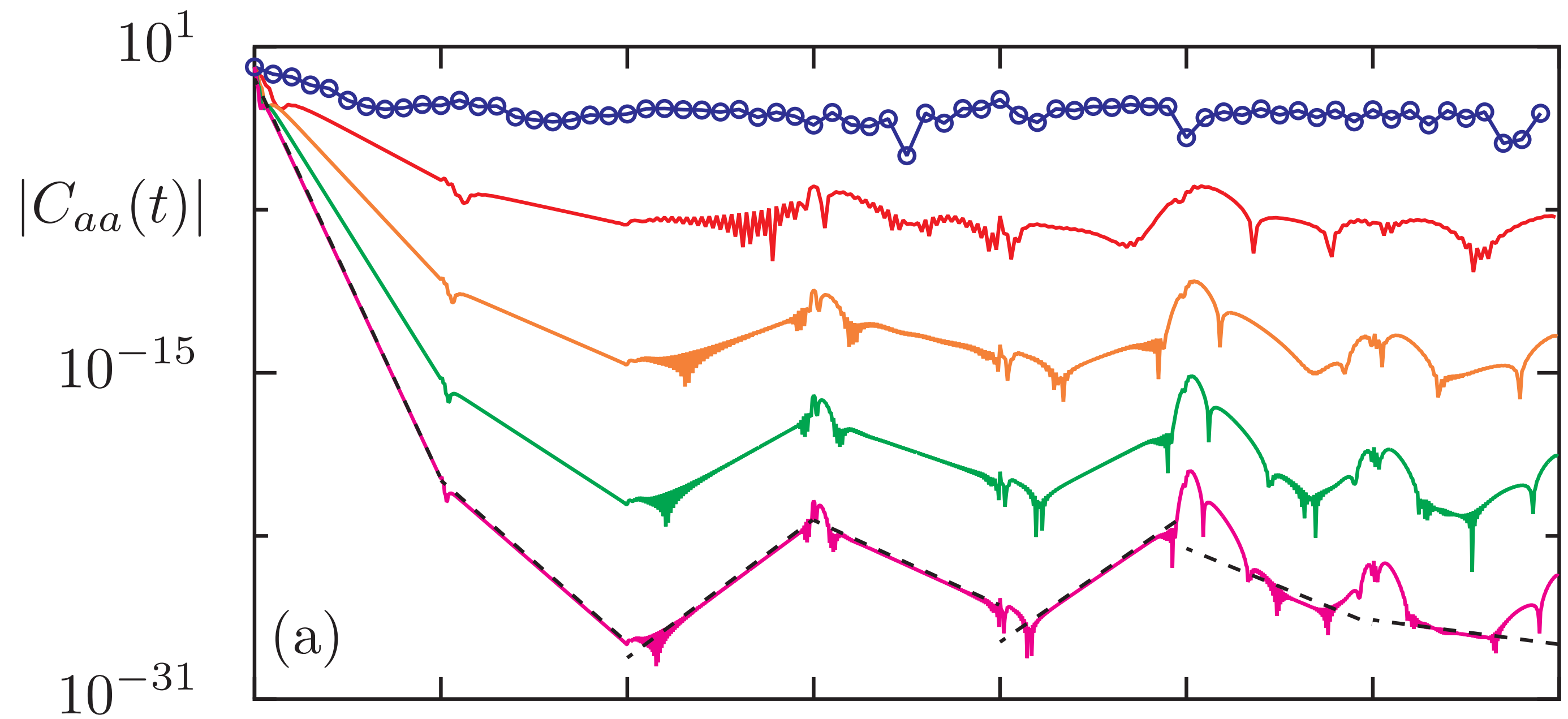


FIG. 3. Probability $p(|\lambda_0(\tau + 1)| > |\lambda_0(\tau)|)$, i.e., for the largest nontrivial eigenvalue to grow when advancing from τ to $\tau + 1$ for various q and for both the T-dual and the generic case. Here we use more than 2000 realizations and 500 for the largest accessible values of τ , respectively, from the same ensembles as used for Fig. 1. The maximum system size is given by $\tau + 1 = 11$, $\tau + 1 = 8$, and $\tau + 1 = 5$ for $q = 2, 3, 4$, respectively. In particular, for $q = 2, 3$ the probability is found to be zero, when there is no bar depicted. For $q = 4$, this holds only up to $\tau = 4$ as we compute the leading eigenvalue only up to $\tau + 1 = 5$.

For some rigorous handle, see
[Bertini, Kos, TP, PRX'21]

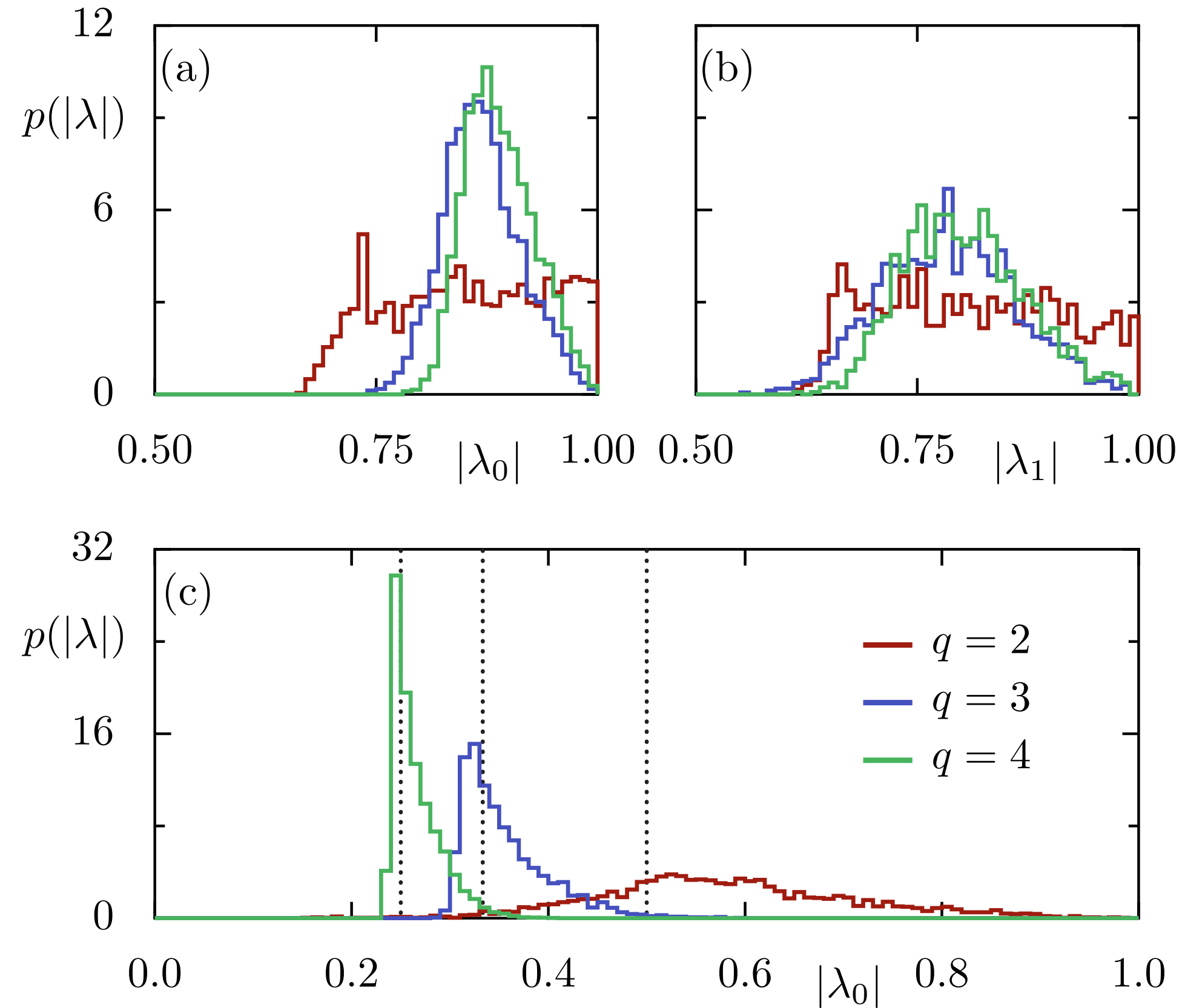


FIG. 1. Distribution $p(|\lambda|)$ of (a) the largest nontrivial eigenvalue λ_0 and (b) the largest relevant eigenvalue λ_1 for T-dual impurity interactions for $q = 2, 3, 4$ (with corresponding τ given by (a) $\tau = 10, 6, 4$ and (b) $\tau = 6, 4, 3$). (c) depicts the distribution $p(|\lambda|)$ of the largest nontrivial eigenvalue λ_0 for generic impurity interactions for $q = 2, 3, 4$ (with corresponding τ given by $\tau = 10, 6, 4$). Dotted lines correspond to $|\lambda_0| = 1/q$. All histograms are created from >1000 realizations with Haar random U in the generic case, and U with Haar random local unitaries u_{\pm}, v_{\pm} and fixed $J = 1/2$ in the T-dual case; see Eq. (11).

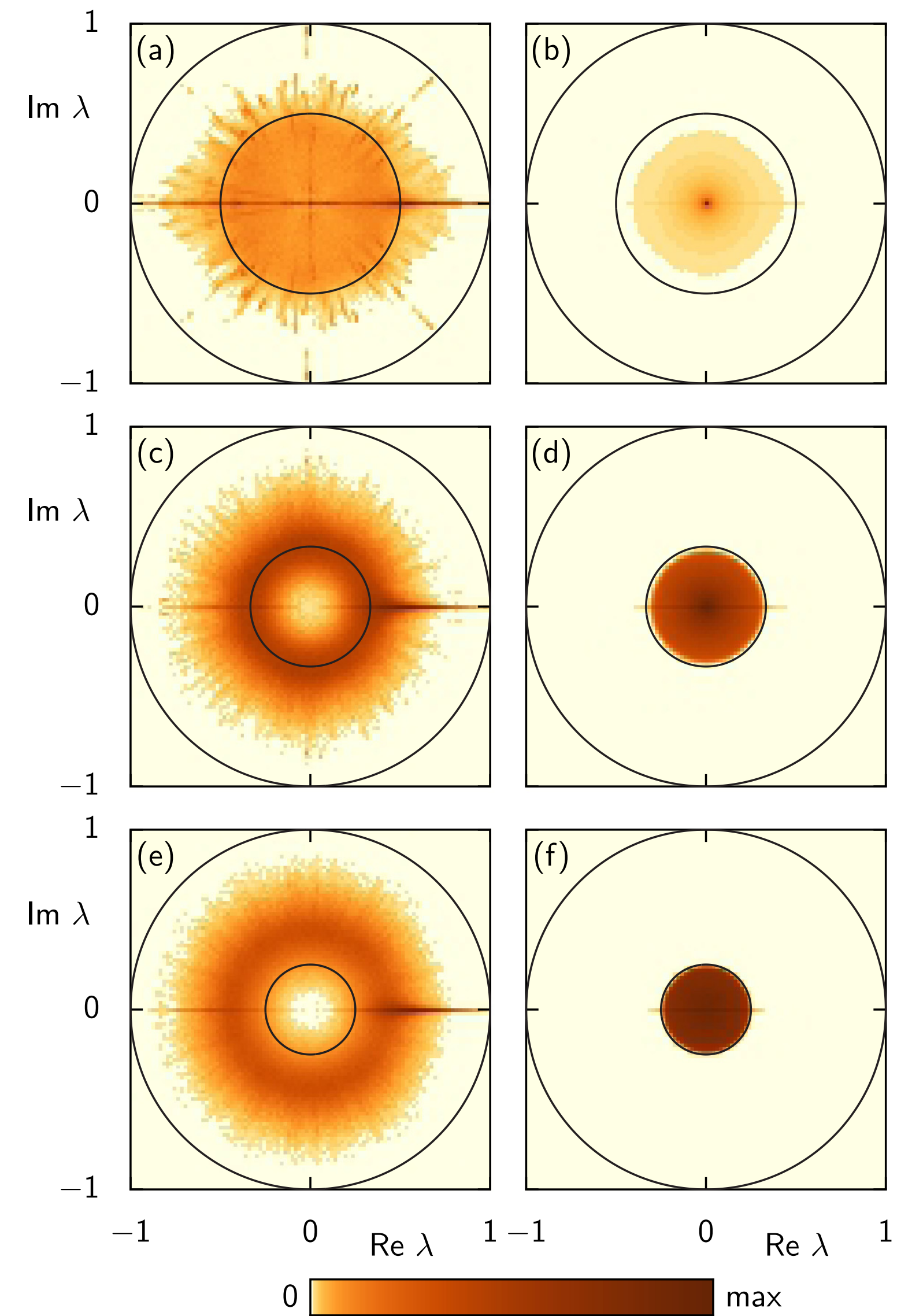


FIG. 6. Histogram of the nontrivial eigenvalues for $q = 2, \tau = 7$ (a), (b), $q = 3, \tau = 4$ (c), (d), and $q = 4, \tau = 3$ (e), (f) for the T-dual case (a), (c), (e) as well as the generic case (b), (d), (f) for 500 realizations of the circuit for each case. The black circles have radii 1 and $1/q$, respectively. Each eigenvalue is weighted by the degree of its degeneracy in the T-dual case and by the dimension of the corresponding Jordan block in the generic case.

see also: F. Fritzsche and TP, arXiv: 2312.12452

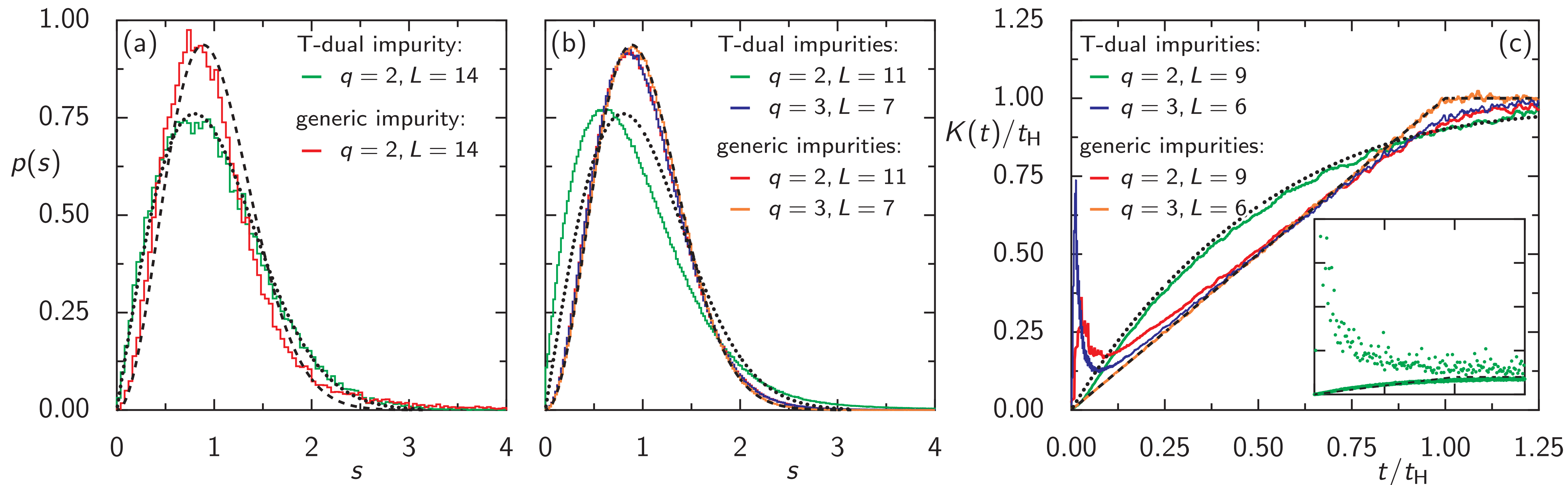
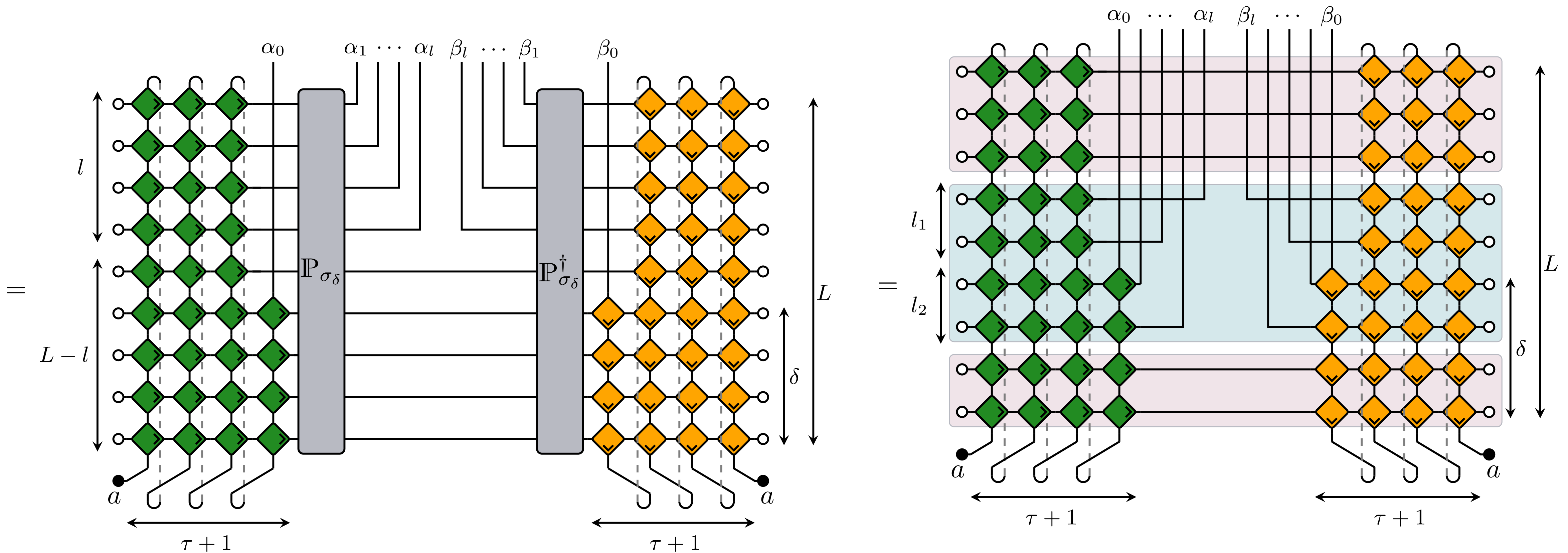


FIG. 5. Level spacing distribution $p(s)$ for (a) the systems shown in Fig. 2 and (b) for the ensemble average over Haar-Random generic impurities and T-dual impurities at fixed $J = 1/2$ and Haar-random local unitaries u_{\pm} and v_{\pm} , see Eq. (11). The dashed black line corresponds to the RMT result for the CUE and the dotted black line to the COE. Panel (c) depicts the normalized spectral form factor averaged over 1000 realizations of impurities. The data are further smoothed by a moving average over a window of 20 time steps. For the T-dual case with $q = 2$ times $t = \tau L$ are excluded from the moving time average. The inset shows the spectral form factor for T-dual impurities with $q = 2$ without smoothing. Black lines indicate the respective RMT spectral form factor with the dashed lines corresponding to the CUE and dotted lines corresponding to the COE. Time and $K(t)$ are scaled by the Heisenberg time $t_H = q^{L+1}$.

Entanglement dynamics

Reduced density matrix (for bipartition $[0, l] + [l+1, L+1]$)

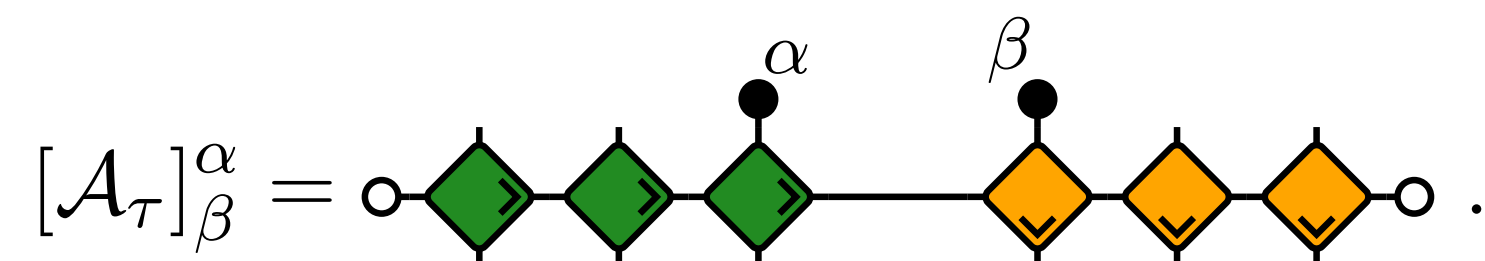
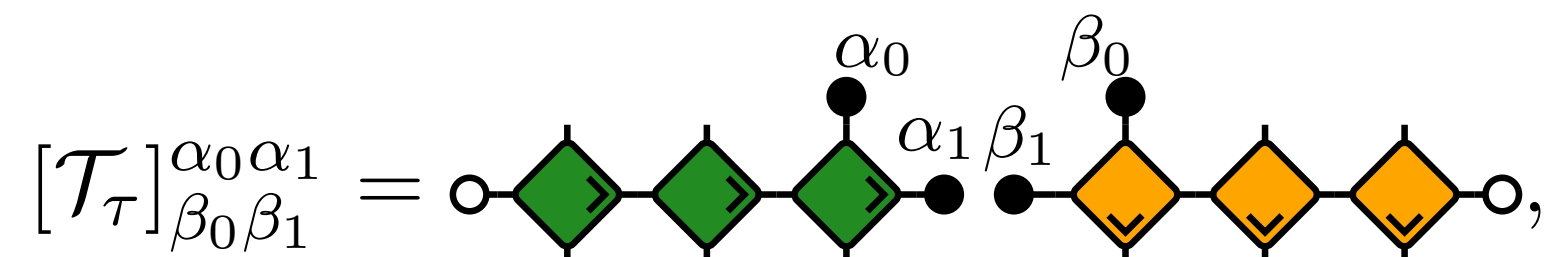
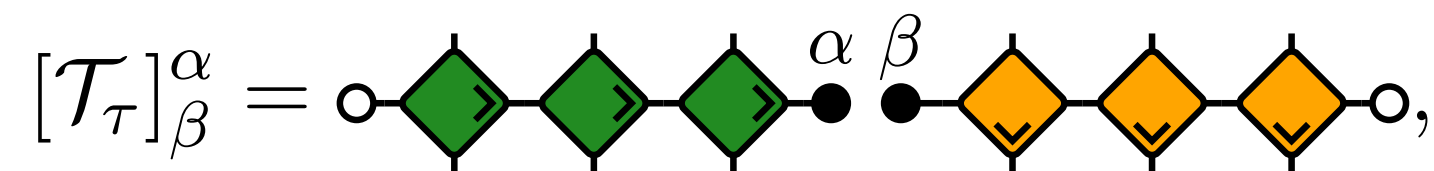
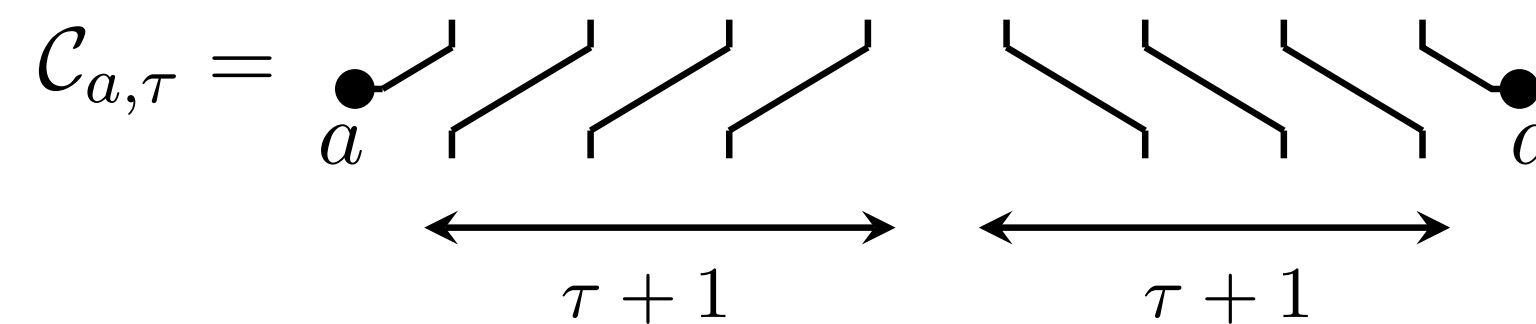
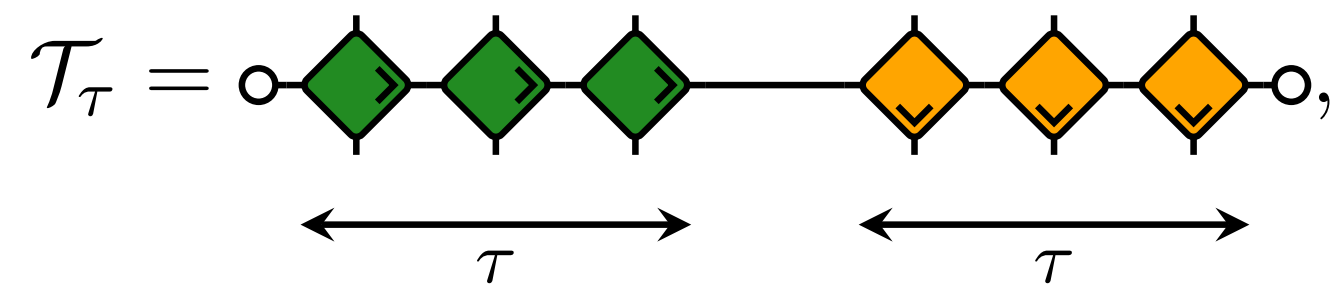
$$\rho_l(t) = \sum_{\alpha_0, \dots, \alpha_l=0}^{q-1} \sum_{\beta_0, \dots, \beta_l=0}^{q-1} \rho_{\beta_0 \dots \beta_l}^{\alpha_0 \dots \alpha_l}(t) |\alpha_0 \dots \alpha_l\rangle \langle \beta_0 \dots \beta_l|$$



Transfer matrix formulation of Renyi entanglement entropies

$$\rho_{\beta_0 \dots \beta_l}^{\alpha_0 \dots \alpha_l}(t) = \text{tr} \left(\mathcal{T}_\tau^{L-\delta-l_1} [\mathcal{A}_{\tau+1}]_{\beta_0 \dots \beta_l}^{\alpha_0 \dots \alpha_l} \mathcal{T}_{\tau+1}^{\delta-l_2} \mathcal{C}_{a,\tau} \right)$$

$$[\mathcal{A}_\tau]_{\beta_0 \dots \beta_l}^{\alpha_0 \dots \alpha_l} = \begin{cases} [\mathcal{T}_{\tau-1}]_{\beta_l}^{\alpha_l} \cdots [\mathcal{T}_{\tau-1}]_{\beta_4}^{\alpha_4} [\mathcal{T}_{\tau-1}]_{\beta_2}^{\alpha_2} [\mathcal{T}_\tau]_{\beta_0 \beta_1}^{\alpha_0 \alpha_1} \cdots [\mathcal{T}_\tau]_{\beta_{l-1}}^{\alpha_{l-1}} & l \text{ even} \\ [\mathcal{T}_{\tau-1}]_{\beta_{l-1}}^{\alpha_{l-1}} \cdots [\mathcal{T}_{\tau-1}]_{\beta_4}^{\alpha_4} [\mathcal{T}_{\tau-1}]_{\beta_2}^{\alpha_2} [\mathcal{T}_\tau]_{\beta_0 \beta_1}^{\alpha_0 \alpha_1} \cdots [\mathcal{T}_\tau]_{\beta_l}^{\alpha_l} & l \text{ odd.} \end{cases}$$



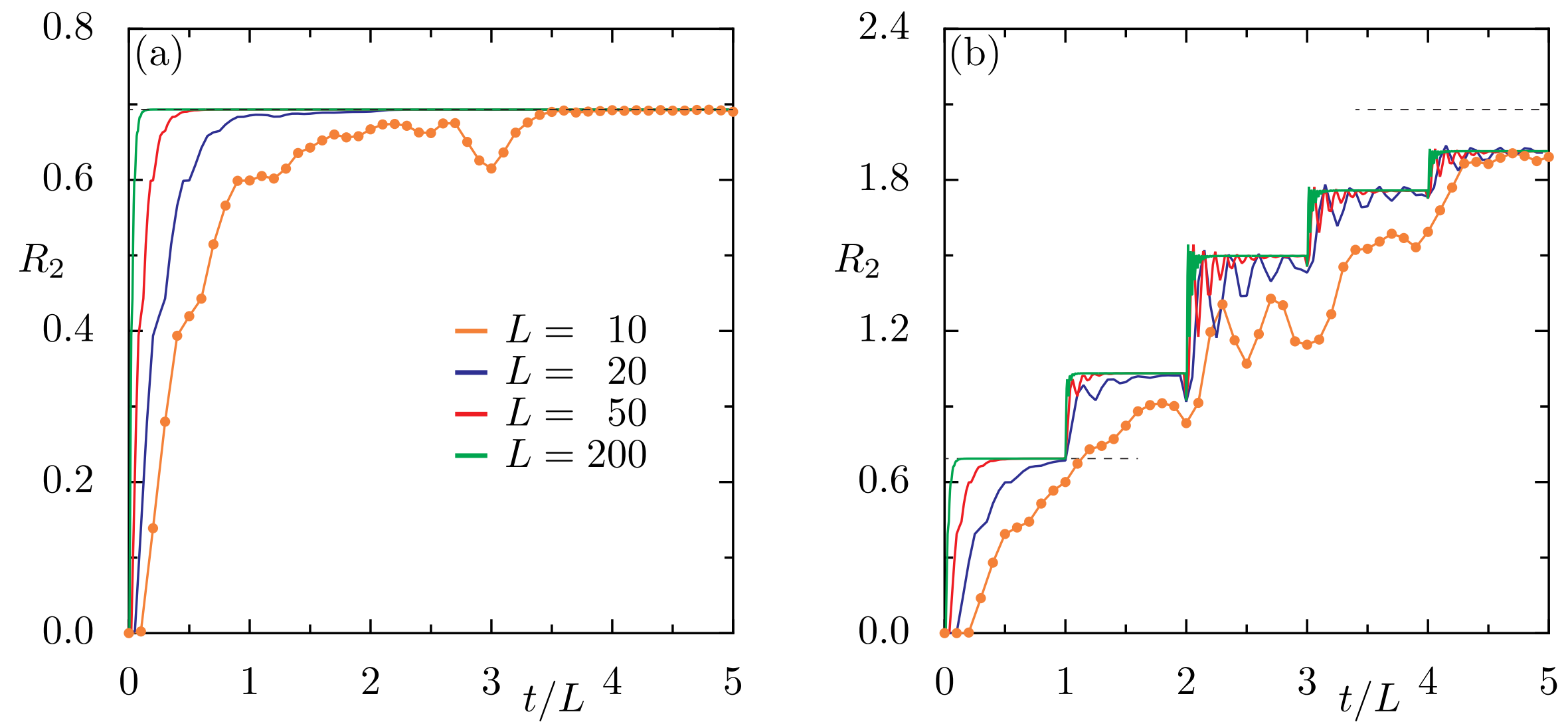


Figure 2: Second Rényi entropy for $q = 2$ and $J = \pi/4 - 0.05$ in Eq. (42) with (a) $l = 0$ and (b) $l = 2$ for a T-dual impurity interaction for various system sizes. (a) The dashed line corresponds to the maximum entropy given by Eq. (63). Orange dots depict R_2 obtained from a direct computation via Eq. (14).

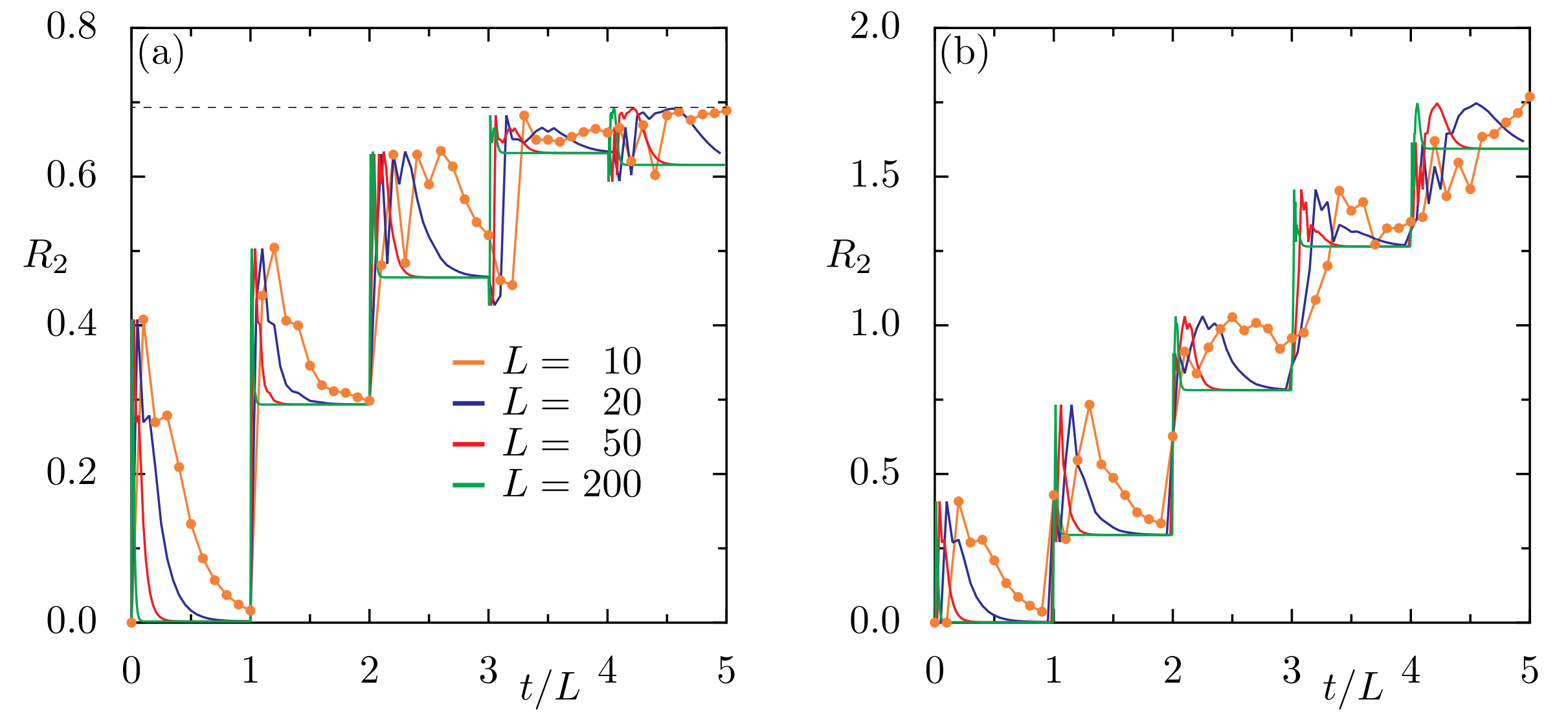


Figure 3: Second Rényi entropy for $q = 2$ with (a) $l = 0$ and (b) $l = 2$ for a generic impurity interaction for various system sizes. (a) The dashed line corresponds to the maximum entropy $(l + 1) \ln(q)$. Orange dots depict R_2 obtained from a direct computation via Eq. (14).

Operator-entanglement dynamics

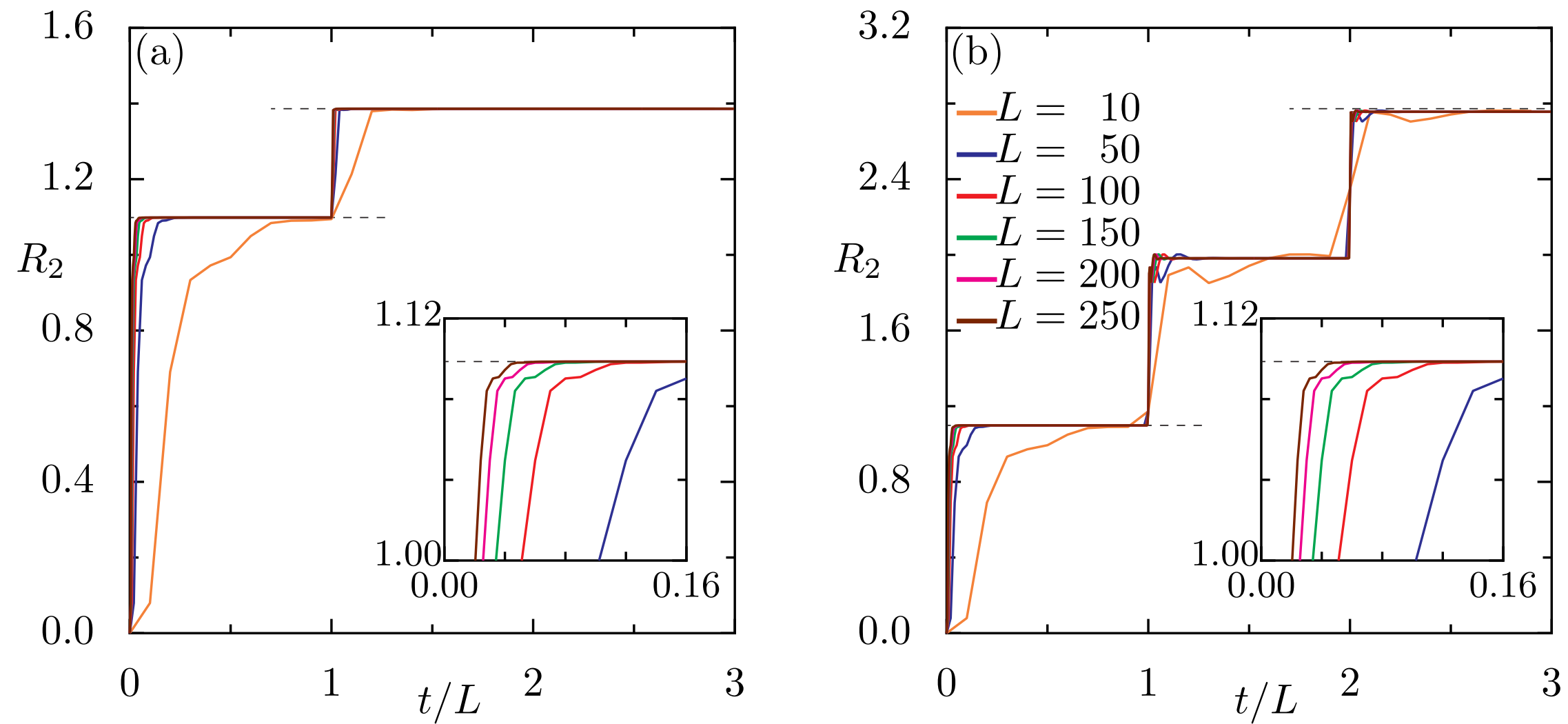


Figure 5: Second Rényi entropy for $q = 2$, a T-dual impurity interaction with $J = \pi/4 - 0.05$ in Eq. (42), and a the spin- z operator with (a) $l = 0$ and (b) $l = 1$ for various system sizes. The dashed lines correspond to (a) Eq. (114) and (b) Eq. (107) as well as the maximum entropy $(l+1) \ln(q^2)$. The inserts show a magnification for initial times.

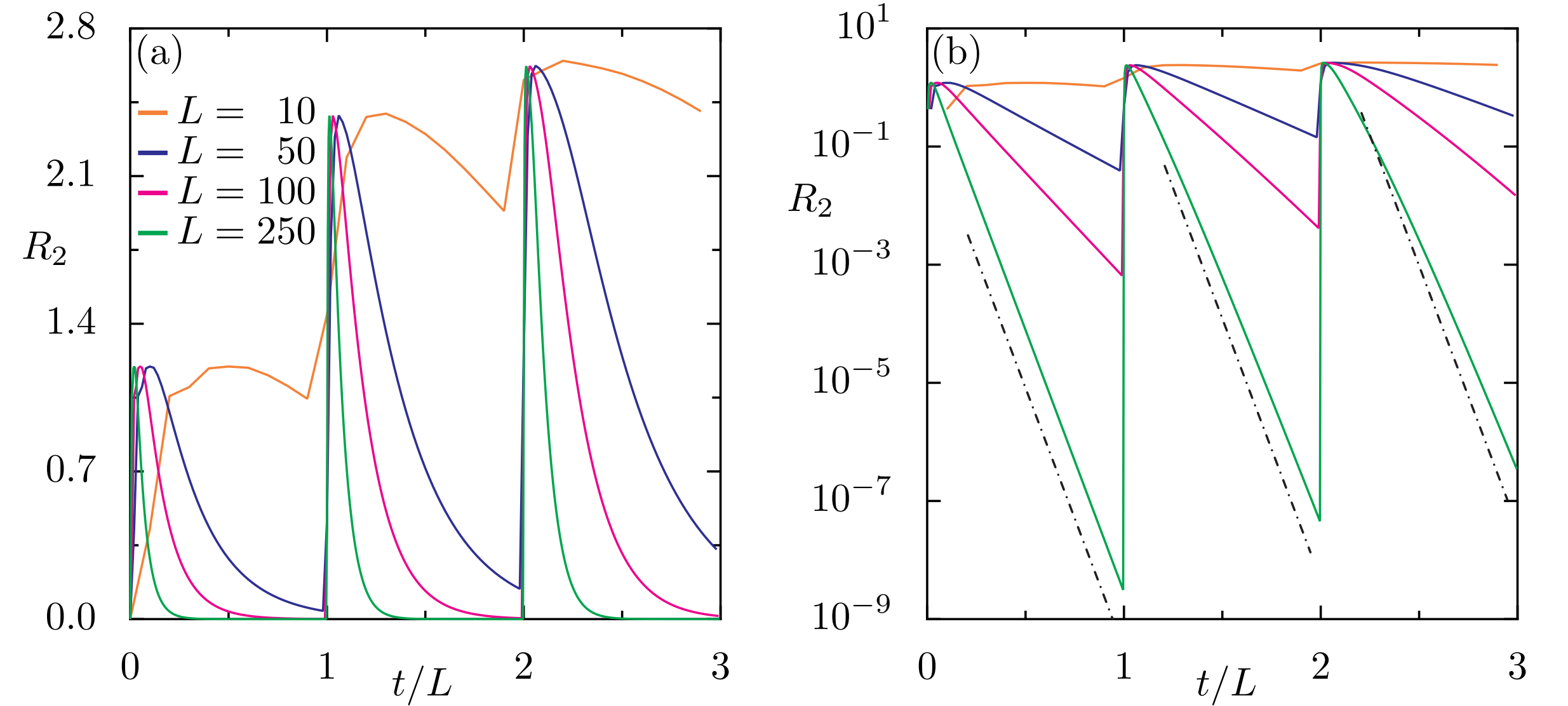


Figure 4: Second operator Rényi entropy for $q = 2$ and $l = 2$ for a generic impurity interaction, a being the spin- z operator, for various system sizes in (a) linear and (b) semi-logarithmic scale. (b) The dash-dotted lines illustrate the asymptotic scaling $|\lambda_0|^\delta$.

Conclusions

1. We introduced minimalist chaotic quantum many-body dynamics akin to chaotic billiards in classical single-particle chaos theory
2. Two “universality classes” of boundary chaos: *T-dual* and *Generic impurity (boundary) interaction*
3. 2-point correlation functions, Renyi-2 entropies (semi)analytically calculated
4. *Future work:* Proving RMT SFF more challenging. Also multipoint time correlators?
Are there quantities which are classically hard (in t for fixed L/t)?